ACSNANO

www.acsnano.org

REVIEW

Precision at Deep Brain: Noninvasive Temporal Interference Stimulation

Shumao Xu,[‖] Han Cui,[‖] Xiao Xiao, Farid Manshaii, Guosong Hong,* and Jun Chen*

Cite This: https://doi.org/10.1021/acsnano.5c15238

Read Online

ACCESS | Metrics & More | Article Recommendations

ABSTRACT: Temporal interference (TI) electrical stimulation is promising for noninvasive neuromodulation with the potential advantages of deep brain targeting. This technique uses high-frequency electric fields applied transcranially, which intersects within the brain to generate a low-frequency modulation field. This intersection enables precise, noninvasive targeting of deep brain regions, addressing a major limitation of typical noninvasive neuromodulation methods, which often yield scattered effects and reduced precision in deep tissue. Recent advances in TI stimulation, supported by computational models and behavioral studies, have demonstrated efficacy in targeting the hippocampus and modulating neuronal activity without notably affecting cortical regions. Its noninvasive nature, coupled with high energy efficiency and precision, positions TI stimulation as a potential tool for activating deep brain regions crucial for behavior and cognition. This review explores the recent developments in TI stimulation, highlighting its mechanisms and pivotal role in precise, noninvasive neuromodulation. The potential of TI stimulation in treating neurological and psychiatric disorders is emphasized, setting the stage for future advances in neurotherapy.

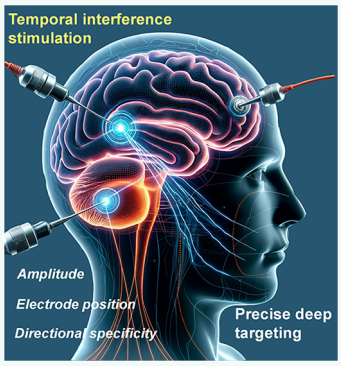

KEYWORDS: *noninvasive neuromodulation, temporal interference stimulation, deep brain regions, precision at deep brain, neurotherapeutic applications*

INTRODUCTION

Neuromodulation has advanced remarkably over the past few decades, offering a promising alternative for managing a wide range of disorders, including depression, Parkinson's disease, chronic pain, obsessive-compulsive disorder, and treatment-resistant epilepsy.[1−11] This approach modulates neural activity directly through physical interventions like electrical or magnetic stimulation and chemical methods like targeted drug delivery, representing a major advance over conventional pharmacological treatments, which typically rely on oral or systemic drug administration.[1,12,13] These treatments often come with side effects, including gastrointestinal distress, cognitive impairment, and systemic toxicity, and often cannot target the neural pathways involved in the disorder, providing transient relief without addressing the underlying disease mechanisms.[14] In contrast, neuromodulation directly targets and modulates specific brain areas, allowing for precise modulation and offering a targeted, lasting effect. The ability to intervene directly at the neural source represents a shift toward personalized and effective treatment strategies in neurology and psychiatry.

Advances in neuromodulation have deepened our understanding of brain function and dysfunction and have driven the development of implantable neural interfaces, including electrocorticography (ECoG) grids, microelectrode arrays (MEAs), and deep brain stimulation (DBS) electrodes.[12,13,15−18] Parallel progress in neuroimaging has provided essential complementary tools, with positron emission tomography (PET) enables in vivo assessment of metabolic dynamics and neurotransmitter activity, while functional magnetic resonance imaging (fMRI) maps brain activity by measuring blood-oxygen-level-dependent (BOLD) signals that reflect neurovascular coupling. Optical imaging techniques such as near-infrared luminescence and bioluminescence, extensively used in preclinical models, allow visualization of cellular and molecular processes within neural circuits and have contributed to linking structural substrates with functional outputs.[19−23] Translationally, DBS has emerged as a clinically established neuromodulation approach, in which electrodes are stereotactically implanted to deliver targeted electrical stimulation to deep brain nuclei[1,2,24,25] (Figure 1A). DBS is approved by the U.S. Food and Drug Administration for Parkinson's disease and obsessive−compulsive disorder,[1,2,26]

Received: September 4, 2025
Revised: November 4, 2025
Accepted: November 5, 2025

Downloaded via UNIV OF CALIFORNIA LOS ANGELES on November 18, 2025 at 08:42:17 (UTC).
See https://pubs.acs.org/sharingguidelines for options on how to legitimately share published articles.

© XXXX American Chemical Society

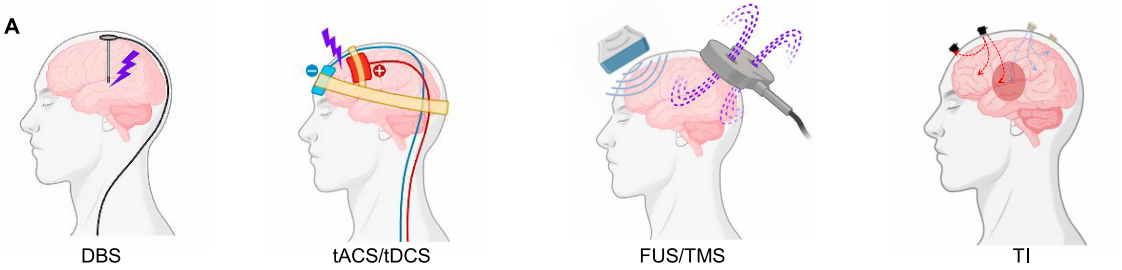

	DBS	tDCS	tACS	TMS/FUS	TI
Frequency	100–180 Hz	0 Hz (constant)	1-100 Hz	1-25 Hz (rTMS) 0.2-1.5 MHz (FUS),	1-10 kHz
Depth	5-10 cm	0.5–3 cm	0.5–2 cm	≤3 cm for TMS, ~15 cm for LIFUS	3-8 cm (non-invasive)
Resolution	1–2 mm^3 (focal)	≥30 mm^3 (diffuse)	3–5 cm^2 (diffuse)	5–20 mm^3 (TMS), ~1 mm^3 (FUS)	5–10 mm (adjustable)
Mechanism	High-frequency inhibition of pathological circuits	Subthreshold polarization of membrane potentials	Entrainment of neural oscillations	Ultrasound/magnetic pulses depolarize neurons	Low-frequency envelope from interfering high-frequency fields
Safety	Surgical risks (hemorrhage, infection, 1–3%)	Mild cutaneous tingling (35% incidence), headache	Similar to tDCS; lower cutaneous irritation risk	Scalp pain, headache/thermal injury risk	Low intensity (≤1.5 mA) avoids cutaneous irritation and tissue heating

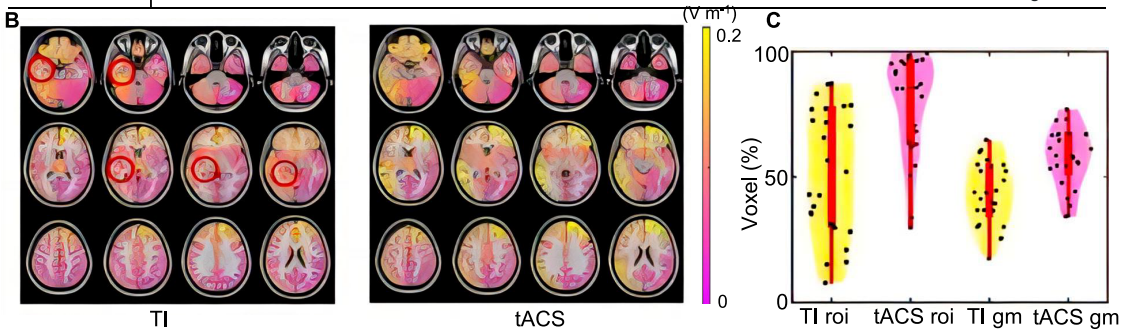

Figure 1. Overview of neurostimulation techniques. (A) Schematic representation of neurostimulation methods: DBS, TMS, FUS, tACS/tDCS, and TI. LIFUS, low-intensity focused ultrasound. (B, C) Comparative analysis of TI and tACS. (B) Simulations of electric fields using the Montreal Neurological Institute (MNI) standard brain model, specifically targeting the hippocampus with TI and tACS techniques. (C) Comparisons of field strength across the regions of interest (ROIs) and the broader gray matter (GM), reproduced from ref 44. Available under a CC-BY 4.0. Copyright [2021] [Springer Nature].

and ongoing investigations are expanding its potential indications to Alzheimer's disease and treatment-resistant depression.[27,28] Nonetheless, as an invasive neurosurgical procedure, DBS carries risks including infection and intracranial hemorrhage, necessitating careful patient selection, long-term follow-up, and comprehensive risk–benefit analysis.[25,29]

To overcome the limitations and risks associated with invasive neuromodulation, a range of noninvasive strategies has been developed, most prominently in transcranial electrical stimulation (tES). This family of techniques includes transcranial direct current stimulation (tDCS), transcranial alternating current stimulation (tACS), and the more recently introduced temporal interference (TI) stimulation.[30−37] These approaches deliver low-intensity electrical fields through surface electrodes placed on the scalp, enabling the modulation of neural activity without the need for surgical implantation. tDCS applies a constant direct current to modulate cortical excitability, whereas tACS delivers oscillatory currents to entrain or disrupt neural rhythms in a frequency-specific manner. Despite demonstrated clinical potential, conventional tES methods are constrained by limited depth penetration, typically influencing only superficial cortical layers within 1−2 cm of the scalp.[38−40]

TI stimulation addresses this key limitation by using two or more high-frequency carrier currents that intersect within the brain to generate a low-frequency envelope capable of modulating neural activity at depth.[41] This mechanism enables focal stimulation of deep brain targets while maintaining noninvasiveness and avoiding the diffuse current spread characteristic of tDCS and tACS. Compared to transcranial magnetic stimulation (TMS), TI offers improved spatial selectivity without requiring bulky coil systems. Although focused ultrasound stimulation (FUS) achieves high spatial precision and deep penetration,[42] its sensitivity to skull-induced attenuation and thermal effects poses safety and

https://doi.org/10.1021/acsnano.5c15238
ACS Nano XXXX, XXX, XXX−XXX

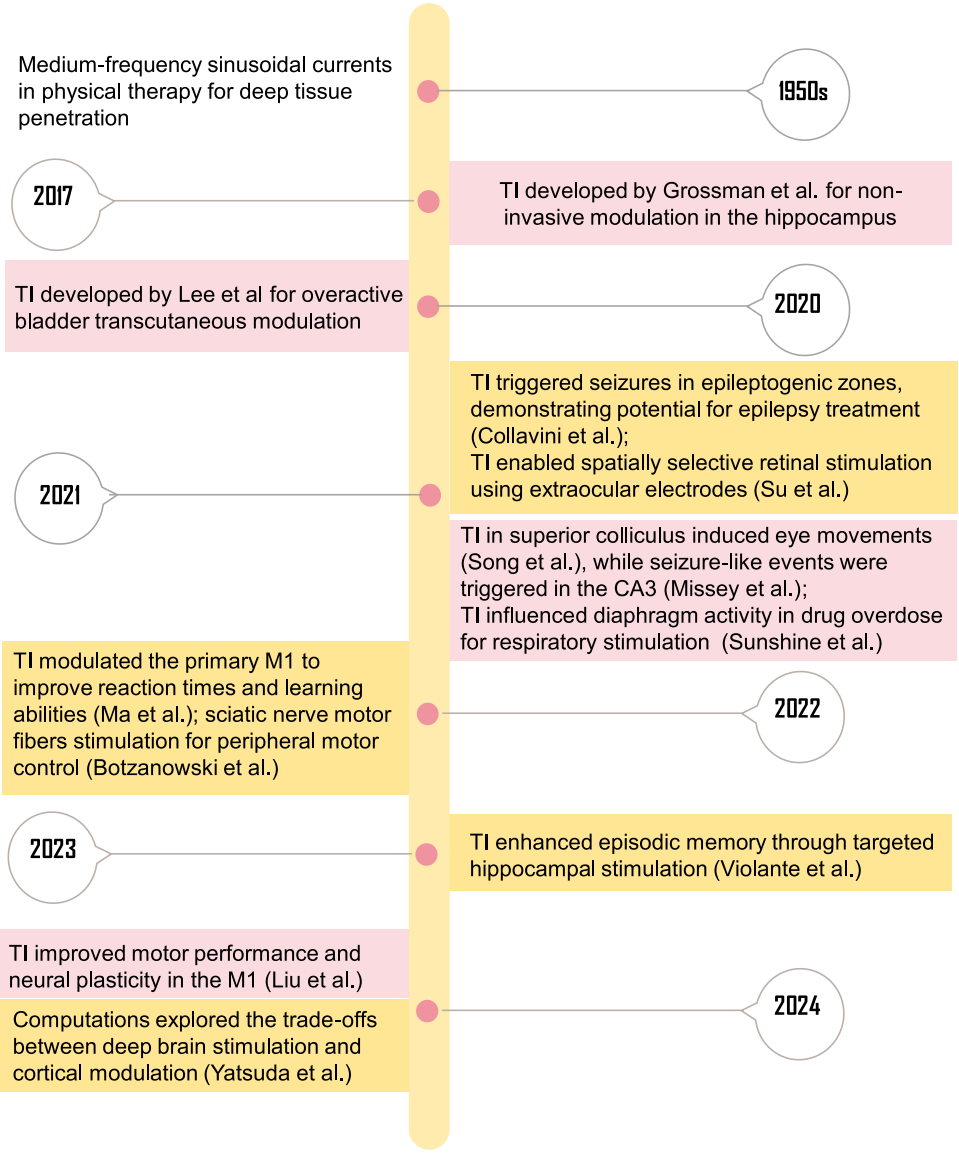

Figure 2. Timeline of milestones in TI stimulation. Red, mouse studies; orange, human trials.

feasibility challenges for repeated clinical use. In contrast, TI provides adjustable depth selectivity through electrode configuration and frequency tuning, while minimizing off-target effects and hardware complexity.[43] This review examines the biophysical principles, computational foundations, and emerging therapeutic applications of TI stimulation. By integrating evidence from modeling studies and early clinical investigations, it outlines the potential of TI to enable precise, noninvasive network-level modulation, positioning it as a promising direction for treatment of neurological and psychiatric disorders.

EVOLUTION OF NONINVASIVE ELECTRIC NEUROMODULATION

TI Stimulation versus tDCS and tACS. TI stimulation offers advantages over conventional transcranial electrical stimulation techniques by combining adjustable depth penetration[37,41,44−46] with the ability to modulate deep brain regions through overlapping high-frequency electric fields. Unlike tDCS, which induces diffuse cortical polarization, or tACS, which primarily entrains superficial oscillations and is limited to cortical modulation,[47] TI generates a low-frequency modulation envelope that can selectively reach subcortical targets such as the hippocampus and striatum with minimal activation of surrounding tissues.[41,43] This spatial precision allows TI to flexibly engage functionally relevant neural rhythms, enabling protocols that entrain hippocampal theta oscillations to enhance memory,[37,38] induce γ-dependent synaptic plasticity,[43] or suppress pathological β rhythms associated with motor disorders.[44] Compared with established noninvasive brain stimulation modalities such as tDCS and TMS, both of which are restricted by shallow penetration depths ($\leq$2 cm) and broad field dispersion, TI demonstrates superior ability to engage deep brain structures including the hippocampus.[48,49] The spatial focusing of TI arises from its use of two or more high-frequency carriers that interfere to generate a focal low-frequency modulation field (Δf = 5−10 Hz), enabling targeted subcortical stimulation with improved selectivity over conventional tACS.[50] Although mean electric field strengths in TI are comparable to those of tACS, TI achieves a more concentrated field distribution (Figure 1B), making it advantageous in clinical contexts where minimizing

https://doi.org/10.1021/acsnano.5c15238
ACS Nano XXXX, XXX, XXX−XXX

Table 1. Overview of TI Stimulation

subjects	technique	intensity	frequency (kHz)	Δf (Hz)	target	outcomes	refs
mouse	cranial electrodes	125 μA	2	10	hippocampus	first TI electrical stimulation	41
mouse	cranial electrodes	1 mA	2	10	superior colliculus	causing eye movements	58
mouse	subdural electrodes	600 μA	1.2	50	CA3 hippocampus	evoking seizure-like events	59
mouse	epidural electrodes	8−10 mA	5	5	diaphragm	respiratory stimulation after drug overdose	57
mouse	transcutaneous electrodes	6.4 ± 1.5 V	2	10	bladder	treating overactive bladder with high penetration and effectiveness.	63
patient	cannula electrodes	1 mA	10	10	epileptogenic zones	triggering spontaneous seizures	61
modeling	extraocular electrodes	1 mA	NA	NA	retina	realizing spatially selective retinal stimulation	62
mouse	cranial electrodes	0.9 ± 0.1 mA	2	3/5/10	primary M1 motor cortex	inducing movements	139
mouse	transcutaneous electrodes	350 μA	3	0.5−4	sciatic nerve	activating motor fibers	65
human	transcutaneous electrodes	2 mA	2	70/20	left primary motor cortex	70 Hz improved reaction time; 20 Hz facilitated learning	177
mouse	cranial electrodes	1 mA	2	10/20	primary motor cortex	improved motor performance; enhanced plasticity	64
human	transcutaneous electrodes	1 mA	2	130	hippocampus	better penetration compared to traditional tACS	93
human	computational modeling	NA	2	10/20	deep brain areas	trade-offs between deep and cortical neuromodulation	69
human	transcutaneous electrodes	0.9 mA cm^{-2} for TI 1:1, 0.45 mA cm^{-2} for TI 1:3	2	5	hippocampus	enhancing memory performance	45
human (PD patients)	scalp Ag/AgCl (4 × 4 HD array)	1.5 mA	2	20	globus pallidus internus (GPi)	40% tremor reduction	66
human (healthy)	transcutaneous bipolar (7 cm^2)	1.0 mA	1.5	5	nucleus accumbens	disrupted reinforcement learning of motor skills	68

off-target cortical effects is essential[38] (Figure 1C). Nonetheless, TI is not without its limitations. Its spatial resolution (~1 cm) remains inferior to that of FUS, which achieves submillimeter precision through acoustic beam focusing.[51,52] Moreover, high-definition tACS (HD-tACS) surpasses TI in cortical applications, producing more localized excitability changes through optimized electrode montages.[51] Achieving cortical modulation with TI often requires higher current intensities, increasing the risk of skin discomfort and reducing tolerability, which constrains its utility for superficial cortical targets. Consequently, TI occupies a unique and complementary niche within the neuromodulation landscape: it is particularly suitable for disorders requiring subcortical precision, such as Parkinson's disease and epilepsy, where human studies have demonstrated clinically meaningful tremor reduction and seizure suppression using subthreshold intensities (<1 V m^{-1}) to avoid adverse sensory effects. By contrast, HD-tACS remains preferable for cortical modulation, and FUS remains the method of choice for ultrafocal stimulation, underscoring the role of TI as a targeted solution for deep, noninvasive neuromodulation.

Historical Evolutions of TI Stimulation. TI stimulation is pivotal in noninvasive brain stimulation, building on the concept of interferential currents recognized in the 1950s.[52,53] Initially, medium-frequency sinusoidal currents were used to achieve a deeper tissue penetration with minimal surface discomfort. A significant advancement came with amplitude-modulated tACS (am-tACS),[54−56] which employed kilohertz carrier frequencies to sculpt low-frequency cortical modulation. This approach laid the groundwork for TI, which extends the principle to deep brain targets by leveraging intersecting high-frequency fields. A breakthrough occurred in 2017 when Grossman et al.[41] introduced the use of two high-frequency currents to generate a low-frequency envelope within the brain, enabling targeted neuronal modulation (Figure 2). By exploiting the neural membrane's inherent high-frequency filtering, TI ensures only the low-frequency envelope interacts with neural tissue, achieving precise deep brain stimulation without invasive procedures. Subsequent research has revealed that TI modulates neural activity through ion-channel-mediated rectification, where voltage-gated channels filter high-frequency inputs into biologically relevant low-frequency signals. These signals selectively tune neuronal excitability based on the ion channel composition and spatial distribution of target neurons, enabling depth-specific neuromodulation.

The evolution of TI stimulation from a theoretical concept to a practical application highlights its versatility and efficacy, as demonstrated by various studies with mouse models and human subjects[41,45,57−62] (Table 1). Initial research in mouse models revealed TI stimulation's ability to precisely activate hippocampal neurons,[41] while subsequent mouse studies explored applications in controlling eye movements,[58] inducing seizure-like events,[59] and modulating respiratory functions.[57] By 2020, preclinical studies demonstrated TI's potential in transcutaneous settings for treating overactive bladder in rodent models, achieving high penetration and effective peripheral nerve modulation.[63] The transition to human trials in 2020−2021 marked a milestone for TI stimulation, with initial studies targeting the primary M1 motor cortex to validate its clinical potential, demonstrating enhanced motor performance and neural plasticity.[60,64] Further research expanded applications to epilepsy treatment through focal modulation of epileptogenic zones[61] and spatially selective retinal stimulation using extraocular electrodes.[62] TI's

https://doi.org/10.1021/acsnano.5c15238
ACS Nano XXXX, XXX, XXX−XXX

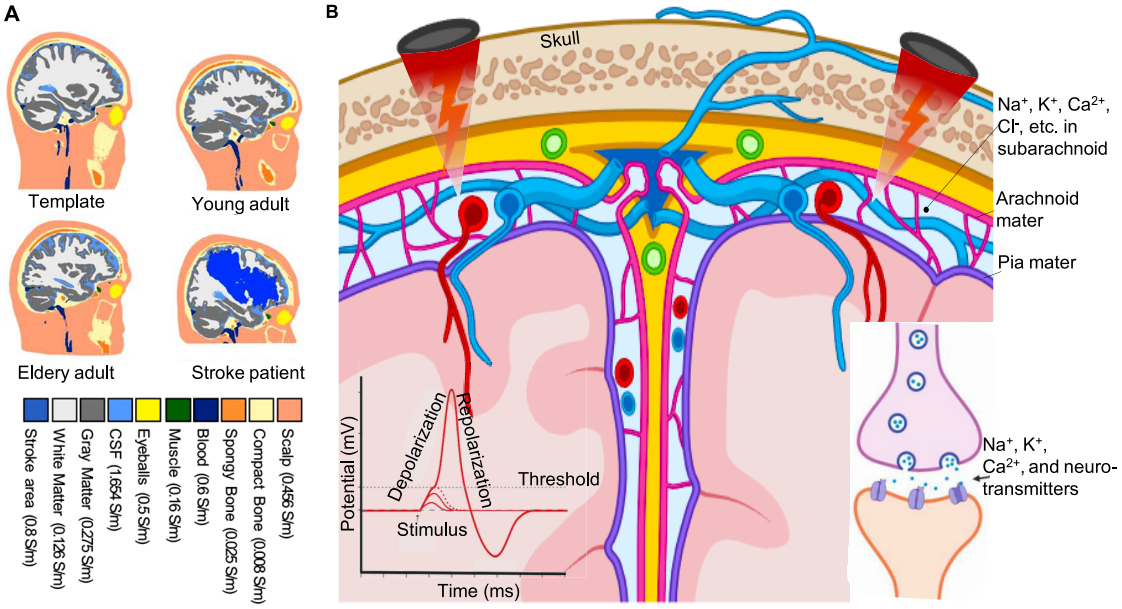

Figure 3. Electric field propagation of TI stimulation. (A) Varying conductivity across different tissue layers in anatomical structures of standard head models, reproduced with permission.[69] Copyright 2024, Frontiers. (B) Biochemical dynamics of TI stimulation in neuronal activation: High-frequency electric fields penetrate the scalp and skull, facilitated by the conductive properties of electrolytes and ions like Na^+, K^+, Ca^{2+}, and Cl^-. The neural membrane responds to this stimulation as ion channels manage the flow of these ions, initiating action potentials and synaptic transmission. Additionally, the induction of electric fields by TI stimulation influences neural activity by interacting with cerebral electrolytes. This interaction alters membrane potential, resistance, and capacitance within the lipid bilayer and protein matrix. The differential conductivity of cerebrospinal fluid and myelinated fibers enhances targeted neuromodulation.

versatility was further evidenced in peripheral neuromodulation, including sciatic nerve activation[65] and respiratory function restoration in opioid overdose models.[57] Beyond motor and sensory domains, TI improved episodic memory *via* hippocampal targeting[45] and showed promise in Parkinson's disease through striatal β-band modulation, reducing tremors, and pathological synchronization.[66] Thalamic TI protocols also restored functional connectivity in essential tremor, offering noninvasive alternatives to surgical interventions.[67] Psychiatric and cognitive applications emerged with TI modulating putamen activity to enhance motor skill learning[68] and prefrontal circuits to alleviate depressive symptoms. Safety and tolerability were underscored in studies addressing cutaneous sensations and optimizing sham protocols, ensuring reliable blinding in clinical trials. Computational models refined parameter selection, balancing depth penetration and cortical sparing for disorders like Alzheimer's and chronic pain.[69] By integrating adaptive algorithms and multimodal biomarkers, TI positions itself as a tool for personalized neuromodulation, bridging gaps in noninvasive deep brain therapy.

BIOLOGICAL PRINCIPLES: SELECTIVE NEURONAL STIMULATION

Despite the skull acting as a barrier to electric fields, especially at low frequencies, its impedance is less restrictive for high-frequency fields. This characteristic allows the high-frequency components of TI stimulation to penetrate the skull effectively and reach deep brain targets with sufficient intensity to induce the desired low-frequency modulation. The varying conductivity across different tissue layers further influences this penetration, as gray matter, white matter, and blood have higher conductivity (1.654 S m^{-1} for blood and 0.275 S m^{-1} for gray matter) than the skull (0.008 S m^{-1} for compact bone and 0.025 S m^{-1} for spongy bone)[69] (Figure 3A).

The biological efficacy of TI arises from the neural membrane's low-pass filtering properties, which render neurons responsive to the low-frequency envelope generated by interfering high-frequency fields. These low-frequency oscillations (e.g., theta, β) modulate synaptic transmission and action potential dynamics by altering neurotransmitter release, receptor sensitivity, and ion channel kinetics[70] (Figure 3B). Low-frequency modulation ($\leq$10 Hz) suppresses neuronal firing in the subthalamic nucleus (STN), mimicking the inhibitory effects of DBS used in Parkinson's disease.[66] This suppression disrupts pathological β synchronization, alleviating tremors without the use of invasive electrodes. Conversely, high-frequency modulation ($\geq$50 Hz) enhances synaptic plasticity in cortical regions, akin to excitatory protocols in tACS.[50] Due to this filtering mechanism, the high-frequency components of TI stimulation penetrate deeply but do not directly activate neural tissue. Instead, the low-frequency envelope, produced by the interference of two high-frequency fields within the targeted area, modulates the neuronal activity effectively. This can enhance the selectivity of neuronal stimulation by exploiting the differential activation thresholds, defined as the minimum stimulation intensity required to depolarize neurons and trigger an action potential, between neurons located in deep brain regions and those in cortical areas. Theta-frequency TI (5 Hz, Δf) entrains hippocampal-cortical networks, enhancing memory consolidation through synchronized oscillations.[71] Similarly, TI-induced β-band modulation (20 Hz, Δf) disrupts pathological synchronization in the subthalamic nucleus, suppressing Parkinsonian tremors,[66] while theta-modulated protocols reduce maladaptive decision-making by destabilizing striatal circuits.[68] Beyond entrainment and disruption, TI enhances synaptic plasticity:

https://doi.org/10.1021/acsnano.5c15238
ACS Nano XXXX, XXX, XXX−XXX

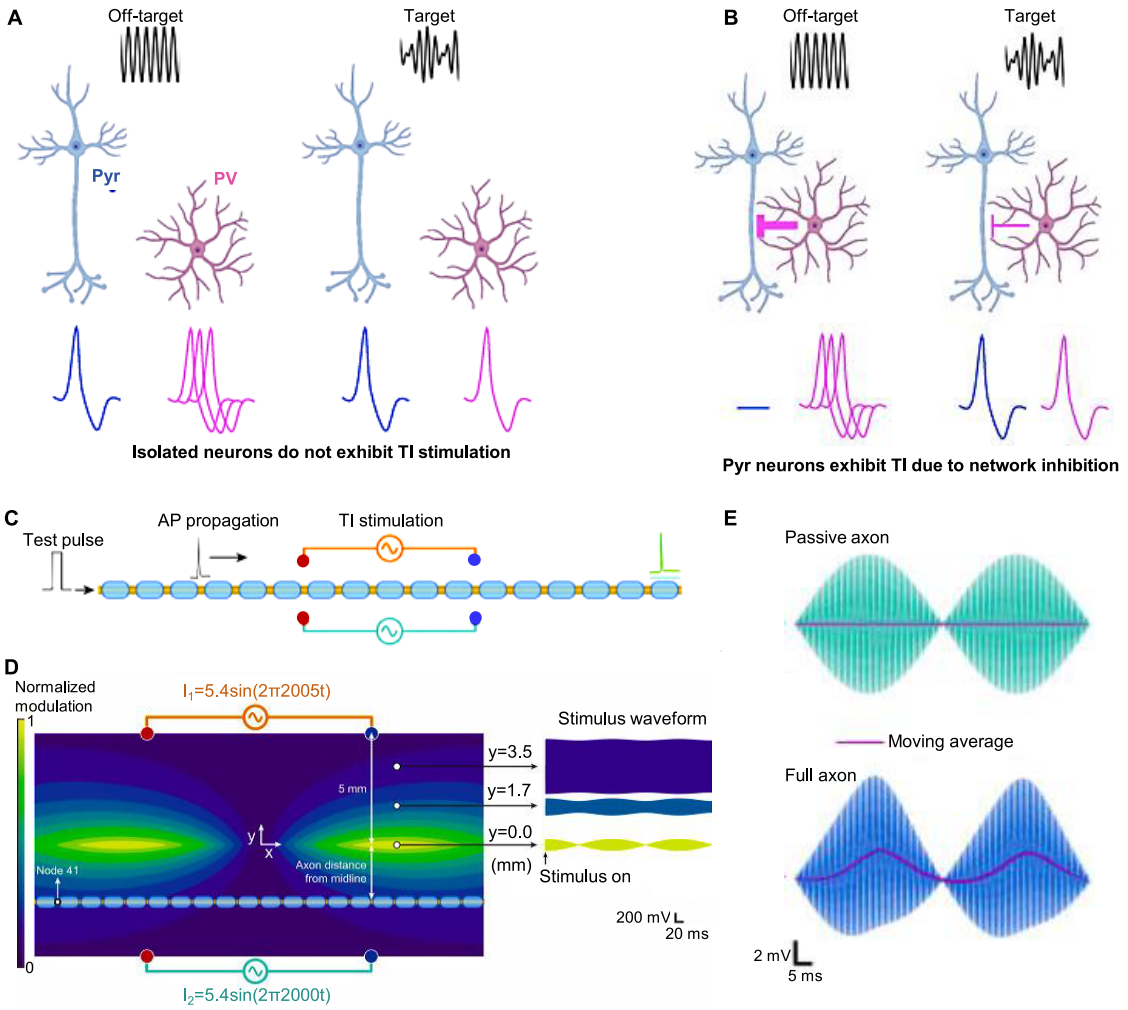

Figure 4. Neuron dynamics and response to TI stimulation: Isolation effects and firing patterns. (A) Isolation effects: Under independent stimulation (no network influence), PV neurons (parvalbumin-positive inhibitory interneurons) in off-target regions fire at high rates under suprathreshold pure sinusoids (high-intensity, direct activation; animal studies), while Pyr neurons (pyramidal excitatory neurons) in target regions synchronize *via* subthreshold modulated sinusoids (low-intensity, network-driven modulation; human studies). (B) Excitatory effects (high-frequency, ≥50 Hz): High-frequency TI enhances Pyr neuron firing through direct depolarization, mimicking tACS-like cortical plasticity. Inhibitory effects (low-frequency, ≤ 10 Hz): Low-frequency TI suppresses PV neuron activity, reducing inhibitory tone and enabling disinhibition of Pyr neurons. In off-target regions, suprathreshold pure sinusoids hyperactivate PV neurons, suppressing Pyr activity. In target regions, subthreshold modulated sinusoids reduce PV-mediated inhibition, enabling Pyr neurons to fire at lower thresholds. Reproduced from ref 78 Available under a CC-BY 4.0. Copyright [2024] [Springer Nature]. (C) Conduction block test: Under suprathreshold stimulation (high amplitude), test pulses at node 0 fail to propagate, indicating conduction block. (D) Activation mapping: Subthreshold amplitude modulation peaks along the axon midline (low-intensity), while extracellular voltages show suprathreshold intensities near electrodes (high-intensity) and subthreshold decay with distance. (E) Axon response: Passive axons (no ion channels) act as low-pass filters, unresponsive to TI. Active axons exhibit subthreshold oscillations (low-intensity modulation) *via* voltage-gated channels. (C–E), reproduced from ref 85 Available under a CC-BY NC-ND. Copyright [2020] [Elsevier].

motor cortex stimulation with γ-modulated TI (50 Hz, Δf) elicits LTP-like plasticity, improving motor learning,[71] and striatal-targeted protocols strengthen corticostriatal connectivity, rescuing dopamine-dependent plasticity in Parkinsonian models.[72] Low-frequency oscillations can enhance or inhibit synaptic strength by affecting the neurotransmitter release and receptor sensitivity.

Additionally, the generation of action potentials can be finely tuned, enabling precise control over neuronal firing patterns. By exploiting differential activation thresholds and neuronal orientation, TI achieves selective neuromodulation, balancing excitation and inhibition to fine-tune neural circuit dynamics. Subthreshold TI protocols, typically applied in humans, modulate excitability without inducing action potentials, relying on synaptic plasticity (e.g., hippocampal theta entrainment for memory consolidation)[71] or task-concurrent coactivation (e.g., motor learning *via* γ-driven plasticity).[73] In contrast, suprathreshold TI, used in animal studies to directly evoke action potentials,[74] risks discomfort and tissue damage in humans. Mechanistically, suprathreshold intensities can induce conduction blocks to silence pathological circuits,[75] while subthreshold regimes require precise parametrization to balance efficacy and safety, as demonstrated in Parkinson's trials, which achieved tremor reduction *via* striatal β modulation.[76] By leveraging frequency-specific interference and differential activation thresholds, TI fine-tunes neural dynamics, offering a versatile tool for disorders demanding depth-specific neuromodulation.

https://doi.org/10.1021/acsnano.5c15238
ACS Nano XXXX, XXX, XXX−XXX

Spatial Configuration of Neurons. The spatial configuration and orientation of neurons relative to the applied electric field influence their activation threshold.[77] Neurons aligned with the electric field's longitudinal axis experience efficient depolarization along their length, making them sensitive to electric stimulation at lower intensities. Pyramidal neurons (Pyr) in the cerebral cortex, which are often aligned with the electric field, can be easily activated. Conversely, interneurons oriented perpendicularly to the electric field, like parvalbumin-positive (PV) inhibitory neurons, require higher stimulation intensities to reach the activation threshold due to less effective depolarization along their length[78] (Figure 4A). The structural organization of neuronal networks in regions such as the motor cortex, where neurons are more uniformly aligned, allows for effective and selective TI stimulation. In contrast, regions such as the hippocampus, with more heterogeneous neuronal orientations, show greater variability in activation thresholds, requiring more precise and higher-intensity stimulation for effective modulation. This structural variance contributes to the differential activation thresholds observed between and within brain regions, thereby affecting the selectivity and effectiveness of TI stimulation in targeting specific neuronal populations.

In isolated conditions, where neurons are stimulated independently, PV neurons in off-target regions respond to pure high-frequency sinusoids with high firing rates, inhibiting Pyr neurons, which fire at lower rates. Conversely, in target regions, modulated sinusoids synchronize the firing of both PV and Pyr neurons, reducing inhibition and allowing Pyr neurons to fire at lower thresholds. When neurons are isolated, most Pyr neurons cease to exhibit TI stimulation (Figure 4A). This phenomenon reveals that the network interactions rather than purely electrical properties govern neuronal responses to stimulation. However, some Pyr neurons still exhibit TI stimulation even in isolation (Figure 4B), indicating that neuronal dynamics and ion channel activity may also play a role. These findings reveal that modulated sinusoids, generated by the interference of high-frequency waves, can induce firing at the modulation frequency, while pure sinusoids alone do not elicit firing. By modulation of the ion-channel-mediated rectification, TI enables selective excitation of neurons based on their ion channel composition and distribution.

Deep brain neurons can respond to the targeted, low-frequency modulation field generated by intersecting high-frequency electric fields,[79] owing to their strategic positioning within interconnected neuronal networks, which facilitate low activation thresholds for synchronous activity. In contrast, cortical neurons, which have varied functions and connections, typically require extensive or synchronized inputs to reach the activation threshold. The physical properties of neurons, including the size of their soma, axons, and dendritic arborization, influence their electrical characteristics and activation thresholds.[80−82] Neurons with large cell bodies or extensive dendritic networks generally require stronger electrical stimuli for depolarization due to their increased surface area and capacitance. Additionally, neurons exhibit unique subthreshold dynamics, largely governed by the kinetics of their ion channels, leading to diverse responses to the same electrical stimulus. Neurons with prominent subthreshold conductances are sensitive to low-intensity stimuli but display variability in reaching the activation threshold due to differences in membrane properties, including ion channel types, densities, and kinetics.[83,84] This variability can be attributed to distinct electrochemical characteristics, including membrane resistance and capacitance, which influence each neuron's response to electrical stimulation.

This subthreshold modulation presents a promising approach for conditions that require gradual, lasting effects, including the enhancement of hippocampal-cortical connectivity in Alzheimer's disease and the stabilization of mood regulation in mood disorders while minimizing the risk of overstimulating the target regions. Leveraging the interactions of neuronal orientation, field geometry, and network connectivity to selectively target specific neural populations while minimizing off-target effects, TI stimulation demonstrates promise for targeted brain stimulation through ion-channel-mediated rectification, selective firing dynamics, and subthreshold modulation.

Electrical Conductivity of Surrounding Tissue. The "sandwich hypothesis" suggests that while TI stimulation effectively targets deep brain regions like the subthalamic nucleus and holds potential for treating Parkinson's disease, it also carries inherent risks of inducing tonic firing or conduction blocks in superficial neural layers.[85] This arises from the inverse distance relationship characteristic of electromagnetic radiation within a conductive medium, where the high amplitudes necessary to reach deep tissues inadvertently impact superficial neurons. In human studies, subthreshold TI protocols modulate the subthalamic nucleus without inducing cortical conduction blocks or tonic firing.[66] Suprathreshold stimulation, which risks discomfort or tissue damage, is restricted to animal models.[48] These effects are further complicated by variability in conductivity across different tissues. Cerebrospinal fluid, which has high conductivity, and myelinated fibers,[86−88] which have relatively low conductivity, influence the distribution and attenuation of electric fields. This variability can alter the efficacy of stimulation and activation thresholds, making it challenging to achieve precise targeting without affecting the surrounding tissues. Moreover, conductivity variations affect the propagation of TI stimulation. Cerebrospinal fluid with a high conductivity enables a consistent distribution of the electric field, potentially improving the efficacy of deep brain stimulation while minimizing the impact on superficial layers. Conversely, myelinated fibers with low conductivity can cause attenuation and scattering of the electric field, complicating the delivery of effective stimulation to the intended deep brain regions.

Furthermore, the neuron's response to TI stimulation extends beyond the previously theorized envelope-based processing.[89−91] Recent findings from firing threshold and undermodulation studies demonstrate that neurons integrate the total amplitude of the stimulation signal, rather than just the low-frequency modulation envelope.[89] Neurons may respond with initial activation, sustain continuous firing throughout the stimulation, or experience conduction blocks, where high-frequency stimuli inhibit the propagation of action potentials. This complexity was demonstrated through conduction block tests[85] (Figure 4C), which determine whether neurons that appear inactive are undergoing inhibition.

Passive and Active Neural Membrane Filtering. The intrinsic properties of neural membranes are pivotal in determining their responsiveness to electrical stimuli, which affects the depolarization level required for triggering action potentials and thus influences activation thresholds.[92] Neuro-

https://doi.org/10.1021/acsnano.5c15238
ACS Nano XXXX, XXX, XXX−XXX

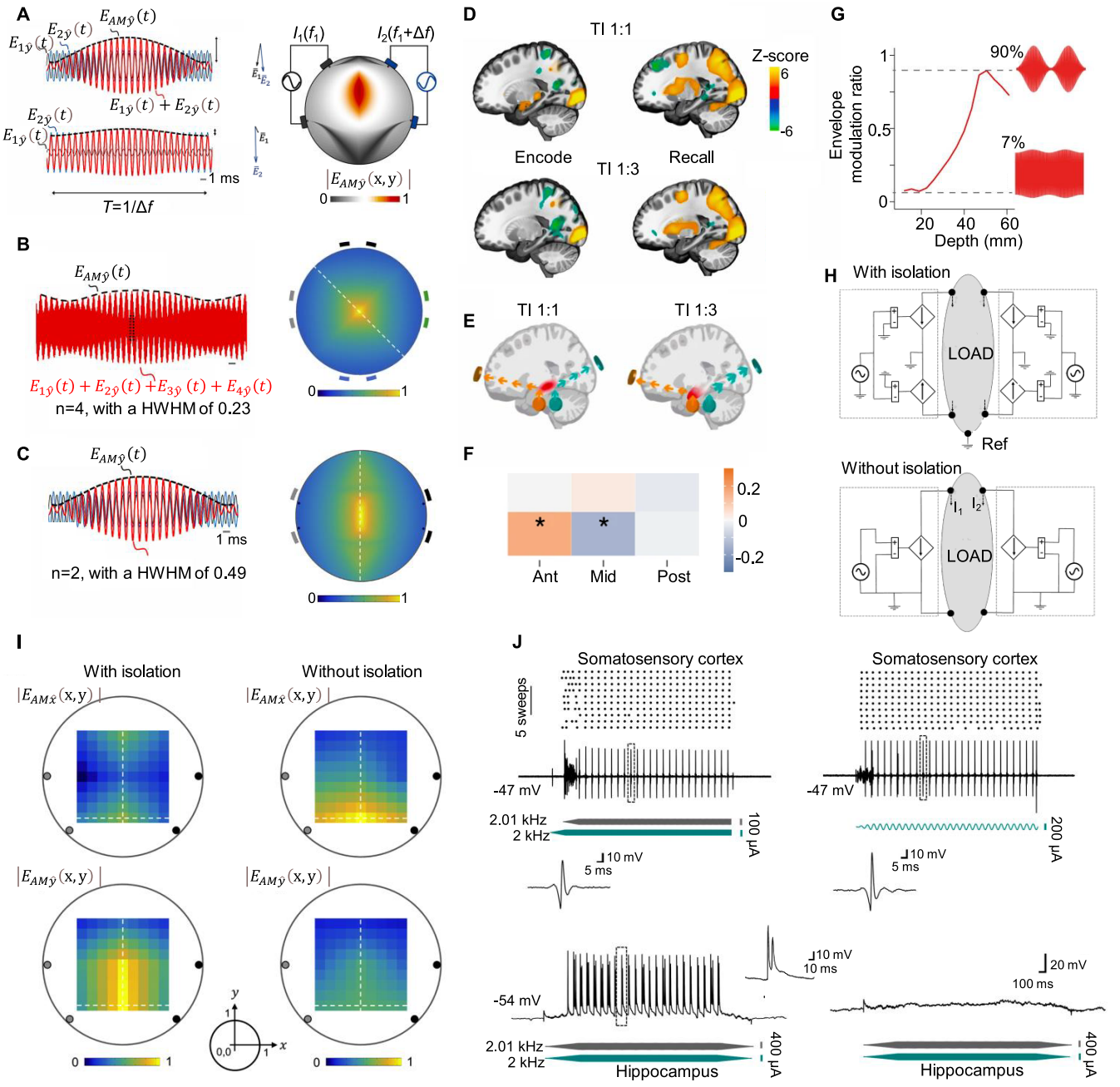

Figure 5. TI stimulation mechanisms: from phantom models to brain activation and connectivity. (A–C) Electric field vectors and envelope modulation. (a) Analysis of electric field vectors E_1, E_2 with magnified views and waveforms, combined envelope $E_{1\hat{y}}(t) + E_{2\hat{y}}(t)$ (red), and modulation $E_{AM\hat{y}}(t)$ (black dashed). The color map shows the spatial distribution of modulation amplitude in the model setup. (B, C) A cylindrical phantom model is stimulated with different numbers of alternating current fields through equally spaced electrodes, producing electric field amplitudes $E_{1\hat{y}}(t)$, $E_{2\hat{y}}(t)$, ..., $E_{n\hat{y}}(t)$ and their cumulative waveform $\sum_{i=1}^{n} E_{i\hat{y}}(t)$ in red. The black dashed line indicates the waveform's envelope, $E_{AM\hat{y}}(t)$, and color maps display the maximal envelope amplitude, $|E_{maxAM}(\hat{x},\hat{y})|$ normalized to the maximum. For $n = 4$, frequencies range from 1.04 to 100 kHz, with a HWHM of 0.23 (B). For $n = 2$, frequencies are 1 kHz and 1.04 kHz, with an HWHM of the main peak at 0.49 (C). (A–C), reprinted from ref 41 Available under a CC-BY 4.0. Copyright [2017] [Cell Press]. (D–F) BOLD signal changes and brain functional connectivity. (D) BOLD signal changes in the brain: TI 1:1 stimulation enhances activity in the left hippocampus during encoding, similar to sham, unlike TI 1:3. (E) Adjusting TI stimulation (1:1 for central, 1:3 for anterior hippocampus) by varying electrode currents for targeted focus control. (F) During encoding, TI 1:3 and 1:1 stimulation reduce FC compared to sham, with TI 1:1 favoring midregion connectivity and TI 1:3 favoring the anterior region. (G) Depth-dependent enhancement of envelope modulation in TI stimulation: Envelope modulation ratio increases with depth. (D–G) Reprinted from ref 45. Available under a CC-BY 4.0. Copyright [2023] [Springer Nature]. (H, I) Stimulator design and focus control. (H) Stimulator with dual channels employs an antiphasic drive for isolation, generating in-phase and antiphase currents, calibrated *via* voltage. A nonisolated version grounds a specific node. (I) High channel isolation in a phantom stimulated at 1 and 1.02 kHz through trapezoidal electrodes sharpens focus, as shown by envelope amplitude maps with peak modulation at the center. Without isolation, modulation spreads, indicating focused versus dispersed effects in high versus low isolation conditions. (H, I) Reprinted from ref 41 Available under a CC-BY 4.0. Copyright [2017] [Cell Press]. (J) Neural responses in the

https://doi.org/10.1021/acsnano.5c15238
ACS Nano XXXX, XXX, XXX–XXX

Figure 5. continued

cortex and hippocampus. Spike raster plots and current-clamp recordings at different amplitudes and durations, reproduced from ref 45. Available under a CC-BY 4.0. Copyright [2023] [Springer Nature].

nal membranes inherently act as low-pass passive filters, attenuating high-frequency signals while permitting the passage of low-frequency signals. Initially, it was hypothesized that TI stimulation exploits these properties by superimposing two high-frequency currents with a slight frequency offset to create a low-frequency modulation pattern that deep neurons can respond to, thereby targeting deep structures without affecting superficial tissues.[41,93]

Recent advances challenge this simplistic passive model, suggesting that active membrane dynamics play a crucial role. Neuronal membranes can actively respond to high-frequency fields, facilitated by ion channels that transform these inputs into usable low-frequency signals.[90,94] This active filtering, involving ion channels like Na^+, K^+, and Ca^{2+}, enables neurons to rectify high-frequency inputs into forms that support neuronal firing but may also introduce high-frequency blocking effects in non-targeted tissues, raising clinical concerns.[92]

Moreover, the composition and distribution of these ion channels affect neuronal excitability. Neurons with a high density of voltage-gated Na^+ channels are prone to depolarize due to a rapid influx of Na^+ ions upon stimulation, thus reducing the external electrical input necessary to reach activation.[95−97] The membrane resistance and capacitance of neurons further influence their firing thresholds. Neurons with high membrane resistance or those close to their activation threshold are responsive to external stimuli, while those with large capacitance need intense or prolonged stimulation to activate.[98]

Investigations into activation dynamics in TI stimulation involve mapping the amplitude modulation of the activating function, which reaches its peak along the midline of the axon[85] (Figure 4D). This mapping illustrates how the effects of TI stimulation vary across different neural pathways, with extracellular voltages showing higher intensities near the electrodes and gradually diminishing farther from the source. The response of axons to TI stimulation also depends on their ion channel composition. In models without active ion channels, axons act as low-pass filters and do not respond to the high-frequency beat frequencies generated by TI[85] (Figure 4E). In contrast, axons with voltage-gated ion channels can detect and respond to the low-frequency envelope produced by TI, even at intensities below the firing threshold. This response results in low-frequency oscillations indicative of subthreshold activity, revealing the crucial role of ion channel dynamics in the rectification and demodulation of TI stimuli.

PHYSICAL PRINCIPLES: ELECTRIC FIELD PENETRATION

The efficacy of TI stimulation relies on the interaction between high-frequency electric currents that converge to generate a low-frequency envelope within the range of neuronal response[41,43,57,99] (Figure 5A). When two high-frequency currents, each with slightly different frequencies, are applied to the brain, they intersect and create an interference pattern. This interference pattern results in a low-frequency envelope that modulates the amplitude of the high-frequency carrier waves. The neurons respond to this low-frequency envelope as it lies within the frequency range that neurons can naturally process.

The choice of high frequencies is critical for noninvasive TI stimulation, as higher-frequency electric fields can penetrate the skull with less attenuation than low-frequency fields due to the dispersive properties of biological tissues. Biological tissues, including bone, tend to attenuate low-frequency signals more than high-frequency ones, making high-frequency currents more effective for deep brain stimulation. As these high-frequency fields intersect within the targeted brain region, their constructive and destructive interference creates a low-frequency modulation envelope capable of stimulating neuronal activity without directly activating neural tissue with high-frequency components. This mechanism allows TI stimulation to selectively target deeper brain structures by adjusting the frequencies and positions of the high-frequency sources, thus creating a focused low-frequency stimulation zone deep within the brain. The resulting electric field from this interaction can be mathematically described by[41]

$$\vec{E}(t) = \overrightarrow{E_1}\sin(2\pi f_1 t) + \overrightarrow{E_2}\sin(2\pi f_2 t) \quad (1)$$

where $\overrightarrow{E_1}$ and $\overrightarrow{E_2}$ refer to the electric field vectors corresponding to the individual high-frequency currents f_1 and f_2, respectively, and t is time. The frequency difference $\Delta f = f_2 - f_1$ produces an envelope modulation at $\Delta f/2$, within the neuronal response range.

Furthermore, the spatial overlap of these high-frequency fields is engineered to ensure that the low-frequency modulation effect is localized precisely at the target location, thus selectively affecting deep brain regions while minimizing influence on the brain's surface or non-targeted areas. Furthermore, the spatial overlap of these high-frequency fields is engineered to ensure that the low-frequency modulation effect is localized precisely at the target location, thus selectively affecting deep brain regions while minimizing effects on the non-targeted areas. This spatial precision is demonstrated through cylindrical phantom model experiments[41,100] (Figure 5B,C), where multiple alternating currents at varying frequencies generate envelope amplitudes that reflect the precision targeting of TI stimulation. The combined modulation of superimposed high-frequency waves can be represented as[101]

$$E_{AM}(t) = 2\cdot\min(|E_1|, |E_2|)\cdot\cos(\pi\Delta f t) \quad (2)$$

where E_1 and E_2 are the electric field vectors corresponding to the individual high-frequency currents, and t is time. $E_{AM}(t)$ is an amplitude-modulated electric field at time t.

The targeting accuracy of TI stimulation is quantified by the half-width at half-maximum ($HWHM$) of the envelope amplitude distribution, which serves as a measure of precision:[45]

$$HWHM = R \times \sqrt{1 - \left(\frac{E_{\max}}{2}\right)^2} \quad (3)$$

where E_{max} represents the maximum electric field amplitude for calculating the spread of the field's peak intensity at half of its

https://doi.org/10.1021/acsnano.5c15238
ACS Nano XXXX, XXX, XXX−XXX

maximum and R is the simplified radius of the elliptical-shaped distribution of an electric field ($R = a^2/b$, a stands for the semimajor axis, and b represents the semiminor axis of the ellipse). Model-based experiments and fMRI BOLD signals, which correlate with synaptic activity rather than direct blood flow,[102] highlight the targeting precision and functional impacts of TI stimulation[45] (Figure 5D). While BOLD signals provide critical insights into synaptic-level modulation, their limited temporal resolution may constrain the detection of rapid neural dynamics. A computational model integrating multimodal fMRI data simulates electrical properties across tissue types during TI 1:1 stimulation (Figure 5E), demonstrating that spatially concentrated modulation fields selectively activate deep brain neurons by accounting for activation thresholds, tissue conductivity gradients, and axonal orientation. This approach effectively targets the primary fiber axis in hippocampal and cortical regions while avoiding unintended cortical activation[65] (Figure 5D,E), underscoring TI's potential for focal neuromodulation in complex neural circuits.

FORWARD AND REVERSE PROBLEMS IN COMPUTATION

While the quasi-static approximation assumes frequency-independent spatial distributions for individual high-frequency fields, the interference between these fields produces a low-frequency amplitude-modulated envelope. The spatial focus of this envelope is determined by electrode geometry, current ratios, and individual anatomical conductivity profiles, as carrier frequencies below 10 kHz remain within the validity range of quasi-static assumptions.[103−105] Consequently, accurate field estimation in TI stimulation requires solving both the forward problem (predicting intracranial field distributions from electrode configurations) and the inverse problem (optimizing stimulation parameters to target specific brain regions while minimizing off-target effects). Addressing these challenges through computational modeling and empirical validation is essential to refine targeting precision, enhance reproducibility, and enable individualized TI protocols for clinical translation.

Forward Problem. The forward problem involves predicting the field distributions and electric potentials in the brain based on stimulation parameters through numerical and analytical methods.[106] Numerical methods, including boundary element methods (BEM) and finite element analysis (FEA) often provide simulations of how electric fields propagate through complex brain geometries. FEA can divide the brain into a mesh of small elements, calculating the electric field in each to create a comprehensive field distribution map. Analytical methods to solve Maxwell's equations in simplified geometrical models also contribute to these predictions. The infinite homogeneous and inhomogeneous cylinder models are used to simulate brain tissue characteristics,[107] where electrode configurations are determined by the length of the electrode arc and the angular orientation corresponding to the brain's anatomy. By approximating each theoretically infinite-length electrode with finite-length segments, the model enhances realism and accuracy, which allows for precise predictions of electric fields and potential distributions in the brain during stimulation, accommodating the complex and varied nature of the brain tissue and electrode placement.

Reverse Problem. The inverse problem in TI stimulation concerns determining stimulation parameters of current intensities, frequency pairs, and electrode configurations that produce a desired intracranial modulation pattern while minimizing off-target activation.,[45,108−111,108] Unlike the forward problem, which predicts electric field distributions from known parameters, the inverse problem proceeds from a defined neurophysiological objective, such as focal modulation of the hippocampus or motor cortex, and computes the parameter set required to achieve it with high spatial specificity. The resolution is central to advancing TI stimulation from conceptual feasibility to precise neuromodulation capable of selectively engaging deep brain circuits without activating surrounding tissues. Computational modeling provides a rigorous framework for solving the inverse problem. Finite element modeling (FEM) enables high-resolution estimation of electric field propagation by discretizing head tissues into anatomically informed mesh elements with heterogeneous conductivities.[60] Through iterative optimization, FEM refines electrode positions and current ratios to concentrate the low-frequency modulation envelope to specific targets. Iterative FEM-based optimization successfully constrained TI fields over the motor cortex by systematically tuning electrode montages and current amplitudes, demonstrating reliable convergence toward focal field distributions. These simulations also quantify trade-offs among focality, depth, and current load, informing parameter optimization strategies for individualized stimulation protocols. Experimental evidence supports the predictive validity of these computational solutions. In vivo studies demonstrated that adjusting carrier frequency differences and electrode geometry can precisely steer the interference envelope toward subcortical structures, such as the hippocampus, without inducing measurable activation in overlying cortical regions.[41] This ability to spatially sculpt neuromodulation fields *via* parameter optimization validates the inverse modeling framework and underscores its translational relevance.

CLINICAL EFFICACY

Preclinical Validation in Animal Models. Preclinical studies in rodent models have established TI stimulation as a promising tool for targeted hippocampal modulation and cognitive enhancement, with particular relevance to memory formation through hippocampal-cortical network interactions. These studies demonstrate that TI stimulation can enhance associative memory, offering potential benefits in cognitive enhancement and treatment for memory-related disorders, as evidenced by improved performance in contextual fear conditioning tasks and increased brain-derived neurotrophic factor (BDNF) expression (+42% after 2 weeks of stimulation)[45,112] (Figure 5F). The mechanistic basis of this potential is supported by precise measurements of electric field envelope modulation amplitudes, which validate the spatial specificity of TI-induced neuromodulation[45] (Figure 5G). Furthermore, the use of electrically isolated current sources ensures accurate and concentrated delivery of stimulation to deep brain structures, addressing a critical challenge in noninvasive neuromodulation[41] (Figure 5H). Isolating stimulation channels allows TI stimulation to focus modulation amplitudes on specific deep brain targets, such as the hippocampus, while minimizing unintended effects on surrounding tissues, a key advancement validated through computational modeling in rodent brain phantoms[41] (Figure 5I). In experimental settings, TI stimulation with a 2 kHz carrier frequency and 5 Hz modulation frequency (Δf) induces

https://doi.org/10.1021/acsnano.5c15238
ACS Nano XXXX, XXX, XXX−XXX

Table 2. Translational Alignment of Key TI Stimulation Metrics

metric	rodent model	human-relevant data	translational implication
stimulation threshold	0.6−0.9 mA (2 kHz carrier)	1.1−1.5 mA (simulated human FEM)	human skull/scalp conductivity requires ∼40% higher current; clinical protocols should adjust accordingly.
target depth	Up to 3 cm (rat brain)	Up to 6 cm (human head model)	deeper penetration in humans due to larger skull volume; optimize electrode array geometry for subcortical targets (e.g., STN).
neuroplasticity response	2-week stimulation: ↑ BDNF (42%)	Ex vivo human slices: ↑ BDNF (29%)	conserved molecular pathway supports potential for synaptic modulation in humans, but magnitude may differ.
safety margin	no tissue damage at ≤1.2 mA (12 weeks)	thermographic data: <38 °C at 1.5 mA (human skin)	initial phase 0 trial threshold: ≤1.5 mA, 30 min/day to balance efficacy and safety.

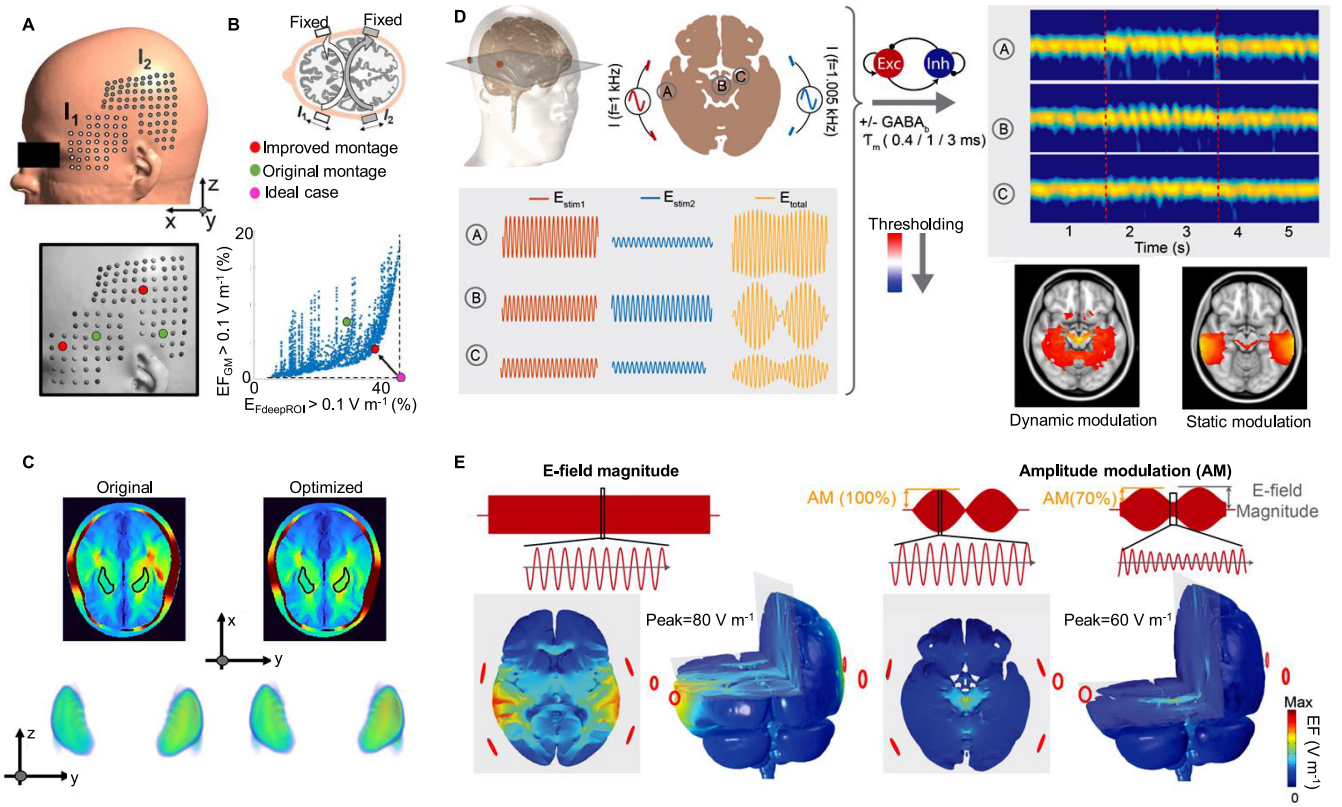

Figure 6. Electrode placement and optimization. (A) Electrode placement optimization on the temporal/parietal side, based on a grid centered on the initial montage position, reprinted from ref 49 Available under a CC-BY 4.0. Copyright [2023] [Springer Nature]. (B) Optimal montage selection by minimizing neuromodulation in GM and maximizing neuromodulation in the deep region of interest. (C) Electric field distributions for selected and original montage configurations across three deep brain regions: putamen, caudate nucleus, and nucleus accumbens. (B, C) Reprinted with permission.[69] Copyright 2024, Frontiers. (D) Multiscale model workflow illustrating the dynamic and static modulation of brain oscillations. Dynamic modulation refers to the time-varying changes in neuronal activity and oscillatory patterns in response to TI stimulation. Static modulation denotes short-term stabilization of γ oscillations relative to baseline without implying lasting plasticity.[144] The model is evaluated under different network parameters, including τ_m (membrane time constant, representing the time scale for neuronal response) and GABA$_b$ inhibition (a specific type of inhibitory neurotransmission involving GABA$_b$ receptors to modulate neuronal excitability). (E) Spatial distribution of electric field magnitude and amplitude modulation along the posterior-anterior axis. (D, E) Reprinted with permission.[93] Copyright 2021, Elsevier.

robust neuronal activation in deep brain regions of rats, with electrophysiological recordings confirming field potentials in the hippocampus and STN at stimulation intensities of 0.6−0.9 mA[45] (Figure 5J). Safety data further support TI's translational potential: 12-week chronic stimulation at ≤1.2 mA shows no histological evidence of tissue damage, and thermographic monitoring confirms scalp temperature elevation remains <0.3 °C.[45] While short-term animal studies demonstrate sustained hippocampal activation and memory enhancement over several weeks, data on long-term efficacy are still emerging, highlighting the need for longitudinal studies in human subjects to evaluate the duration of the effects and optimize repeated or continuous stimulation protocols. Advancing TI stimulation for clinical applications will require refining computational models to improve targeting accuracy, developing adaptive algorithms for real-time modulation that adjust to individual brain responses,[113,114] and incorporating multimodal data to dynamically optimize stimulation parameters.[45,115−119] These advances not only enhance precision and efficacy but also support personalized neuromodulation approaches, which may mitigate the potential adverse effects. Ultimately, long-term efficacy and safety data from well-designed longitudinal studies are pivotal to validating TI stimulation as a sustainable and safe neuromodulation technique for cognitive and neurological disorders.

https://doi.org/10.1021/acsnano.5c15238
ACS Nano XXXX, XXX, XXX−XXX

Human-Relevant Modeling and Translational Considerations. Translational comparisons between rodent and human data indicate that TI stimulation engages conserved neural mechanisms but requires parameter scaling to account for human biophysical constraints. In rodents, effective modulation of hippocampal and striatal circuits is achieved with currents of 0.6−0.9 mA at a 2 kHz carrier frequency, whereas human biophysical simulations indicate that 1.1−1.5 mA is required to generate comparable intracranial electric fields due to increased skull impedance[34,41,68,85,120] (Table 2). This discrepancy arises primarily from anatomical differences, including skull thickness (rodent: ∼0.2 mm vs human: 6−8 mm) and tissue conductivity gradients, which alter current flow and field interference patterns. Despite these challenges, achievable stimulation depth scales favorably: rodent studies demonstrate reliable modulation up to ∼ 3 cm,[7] while 3D FEM simulations in human head models (n = 5 MRI-derived anatomies) predict field interference at depths up to 6 cm, suggesting that subcortical targets such as the subthalamic nucleus and hippocampus remain accessible with optimized electrode montages[45] (Figure 5G). Activity-dependent plasticity mechanisms appear conserved across species, as chronic TI stimulation upregulates BDNF expression in rodent hippocampus (+42%) and ex vivo human cortical tissue (+29%) under analogous stimulation conditions, though the blunted magnitude in human tissue likely reflects species-specific receptor density.[9,121,122] Preclinical safety margins also translate favorably; prolonged stimulation at ≤1.2 mA in rodents induces no histopathological abnormalities,[123] while human thermography confirms scalp heating <38 °C at 1.5 mA, supporting the feasibility of early-stage human testing using conservative dosing (≤1.5 mA, ≤30 min per session).[124−126]

However, several critical gaps need to be addressed before clinical validation. FEM indicates that skull-induced scattering in humans reduces focality by approximately 25% relative to rodent models,[127] suggesting standardized protocols may be insufficient and patient-specific electrode configurations based on individual head models will likely be required. Physiological heterogeneity adds further complexity: neurodegenerative pathology, age-related cortical atrophy, and vascular comorbidities (e.g., hypertension, diabetes) can influence current distribution and neural responsivity,[128] potentially diminishing TI efficacy in clinical populations. Stratification by disease stage and comorbidity profile will therefore be essential in the trial design. To address these challenges, a phased regulatory strategy is necessary, beginning with Phase 0 feasibility studies in healthy volunteers to verify depth targeting using functional MRI, followed by Phase I studies in Parkinson's disease patients to evaluate acute safety and preliminary efficacy.[129,130] Technical advancements are equally critical, including the development of adaptive closed-loop algorithms integrating real-time EEG−fMRI feedback to mitigate variability from arousal fluctuations or pharmacological states,[131−133] and multimodal data integration to enable dynamic parameter optimization.[134,6,135−137] Additionally, longitudinal data are needed to assess the durability of effects and long-term safety regarding neurovascular function and blood−brain barrier integrity.[138] These findings support the mechanistic plausibility of TI for noninvasive deep brain stimulation but underscore the need for individualized approaches to compensate for interindividual variability in cranial conductivity and pathological states.

OPTIMIZING TI STIMULATION FOR TARGETED DEEP ACTIVATION

Electrode Placement and Optimization. The optimization of electrode placement is critical for achieving precise and targeted neuromodulation with TI stimulation, which can ensure that the electric fields generated by the electrodes are directed with high accuracy to the intended deep brain regions, minimizing the spread of the stimulation to nontarget areas.[139] The optimization process typically involves using anatomical templates and computational models to guide the placement of electrodes. A common approach is to position the electrodes on the temporal/parietal regions, using a grid centered on an initial montage position[49] (Figure 6A). This method allows for fine-tuning of the spatial arrangement of electrodes to maximize the focus of the stimulation on regions of interest. A montage refers to the configuration and placement of electrode pairs on the scalp or other superficial regions[69] (Figure 6B), which directly influences the direction and strength of the electric fields applied to the brain. The configuration of the montage is key to ensuring that the stimulation is delivered effectively to the target deep brain regions. By adjusting the spacing and orientation of the electrodes, it is possible to direct the electric field with high precision to the target areas, such as the putamen, caudate nucleus, or nucleus accumbens, while avoiding unwanted stimulation in adjacent cortical regions such as the gray matter. This balance is crucial for achieving the desired therapeutic effects, as improper montage selection could lead to stimulation of nontarget areas, reducing the efficacy of the treatment and potentially causing adverse effects.

Optimal montage selection involves a trade-off between maximizing neuromodulation in deep brain regions and minimizing stimulation in the surrounding cortical regions. By choosing the best electrode configuration, neuromodulation in the gray matter can be reduced by up to 40−50%, while simultaneously enhancing neuromodulation in deep brain areas by as much as 30−800%. Figure 6C illustrates the electric field distributions for the selected montage configurations compared to the original montage, revealing how the optimized placement leads to a significant increase in neuromodulation within the target deep brain regions, with minimal interference in the gray matter.[69] This approach enhances the specificity and efficacy of TI stimulation, making it possible to achieve targeted therapeutic effects while reducing off-target effects.[43,140−143]

The multiscale model workflow integrates computational simulations with experimental data to analyze the effects of TI stimulation at multiple levels of brain organization[93] (Figure 6D). This model allows for an in-depth understanding of how applied electric fields interact with neuronal circuits at the cellular and network levels. The workflow differentiates between dynamic modulation with time-varying changes in neuronal activity in response to the stimulation, and static modulation with short-term stabilization of γ oscillations relative to baseline without implying lasting plasticity.[144] Dynamic modulation is crucial for real-time alterations in neural excitability, allowing for precise control over the timing and synchronization of neuronal firing. This is achieved through the temporal interference of high-frequency electric fields, which generate low-frequency modulation that impacts neuronal firing patterns. To realize dynamic modulation, the electric field applied by TI stimulation interacts with neuronal

https://doi.org/10.1021/acsnano.5c15238
ACS Nano XXXX, XXX, XXX−XXX

Table 3. Comparison of Mediolateral (ML) and Anteroposterior (AP) Stimulation

	ML stimulation	AP stimulation
electrode placement	symmetric electrodes along the medial-lateral axis (e.g., FT7-FT8 in 10−10 system).	electrodes along the anterior-posterior axis (e.g., F3−P3 in 10−10 system).
electrode distance	Wide separation to create lateral fields.	closer spacing along the AP axis for focal stimulation.
orientation	lateral electric field (perpendicular to midline).	longitudinal electric field (parallel to AP axis).
frequencies	β/γ (20−40 Hz) for motor pathways and bilateral connectivity.	theta/α (4−12 Hz) for cognitive networks (e.g., prefrontal cortex, cingulate).
currents	two-channel (I1, I2) with higher intensity for bilateral regions.	two-channel (I1, I2) with lower intensity for deep midline targets.
target regions	motor cortex, somatosensory cortex (superficial bilateral regions).	cingulate cortex, prefrontal cortex (deep midline regions).
penetration	penetration: superficial bilateral cortical areas (without TI); deeper with TI optimization.	deeper midline structures (via TI or optimized tES).
neural pathways	interhemispheric communication, motor circuits.	default mode network, executive/attentional pathways.
applications	motor rehabilitation, bilateral cortical interaction.	cognitive enhancement, mood regulation, attention modulation.

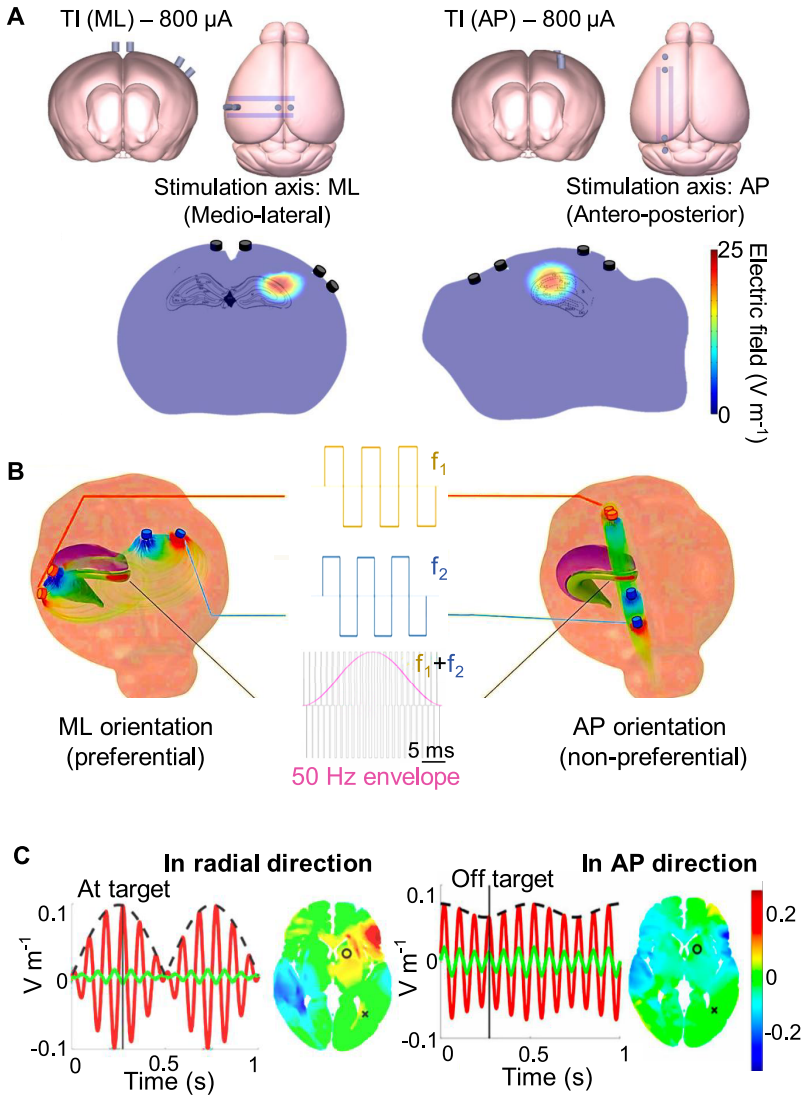

Figure 7. Orientation-targeted electric field modulation in TI stimulation. (A) Two TI stimulation axes with scaled electrode placements: the electric field lines are aligned parallel (ML) or perpendicular (AP) to the Schaffer collaterals. AP, anteroposterior; ML, mediolateral. (B) Orientation-targeted TI with two pairs of electrodes in the hippocampus: ML, aligned with hippocampal axons (preferential), and AP, perpendicular to these axons (nonpreferential). (A, B) Reprinted from ref 59 Available under a CC-BY 4.0. Copyright [2021] [Frontiers]. (C) TI stimulation targeting near the left striatum at a specific time point in radial (red) and AP (green) directions, reproduced with permission.[145] Copyright 2023, Frontiers. Black dashed lines indicate the modulation envelope. The electric field at the target brain region has the maximal effect of TI stimulation. Stimulation is less focused or unintended in off-target regions but still may influence neural activity.

membranes, modulating their excitability in a time-varying manner. This modulation is dependent on the frequency and amplitude of the applied field, with lower frequencies facilitating synchronization of neuronal firing and higher

https://doi.org/10.1021/acsnano.5c15238
ACS Nano XXXX, XXX, XXX−XXX

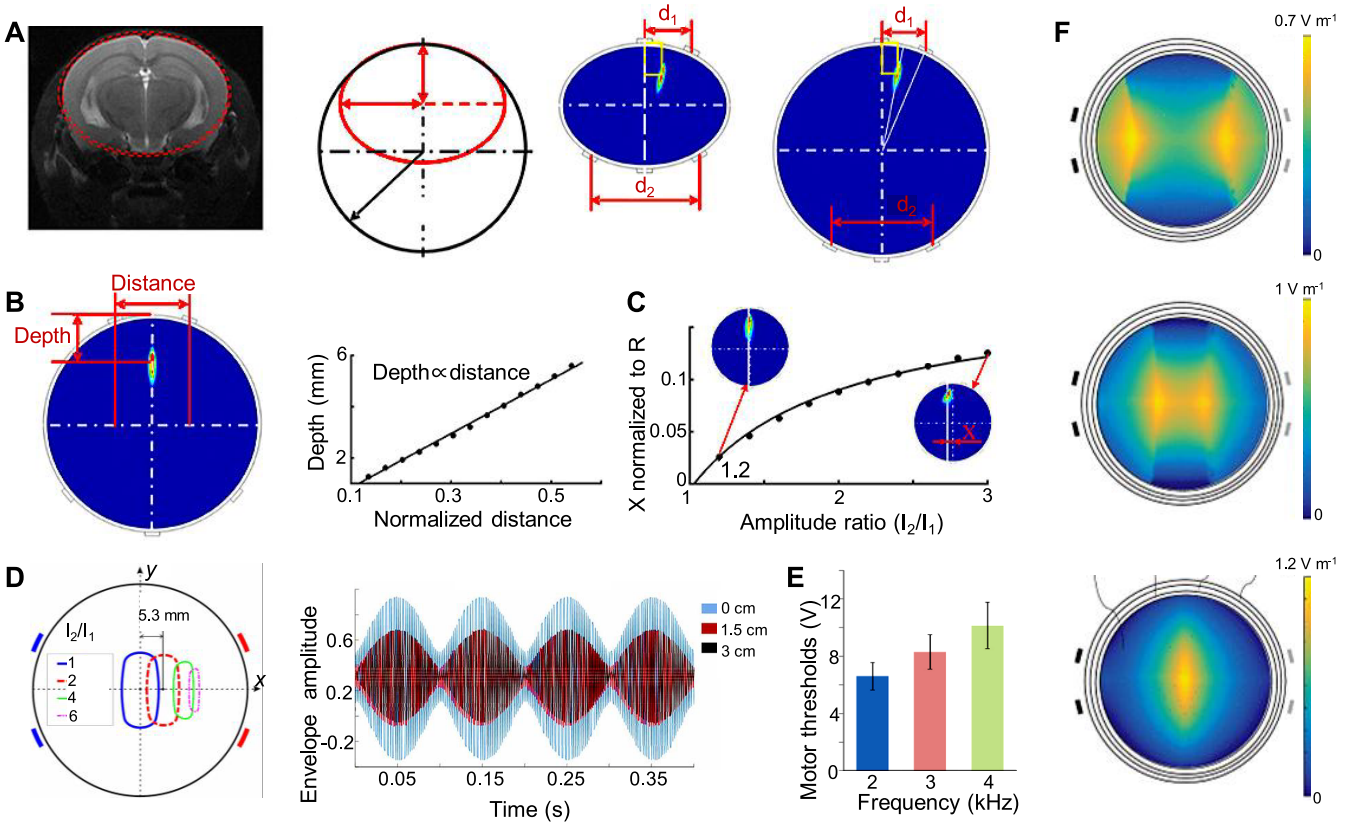

Figure 8. Methodological parameter space in TI deep brain targeting. (A–C) Targeting approach using columnar models, reprinted with permission.[148] Copyright 2020, Frontiers. (A) The elliptic model derived from MRI data and a simplified circular model display distributions of electric field amplitude. (B) Correlation between the target area depth during temporal interference stimulation and the spacing between electrodes on the scalp. (C) The link between the peak position in the electric field and the amplitude ratio (I_1/I_2) within the field's amplitude envelope. (D) Electric field distribution and temporal envelope amplitude at varying depths for a beat frequency (Δf) of 10 Hz, reprinted with permission.[107] Copyright 2019, IOP Science; and with permission.[58] Copyright 2021, IOP Science. (E) Variations in motor thresholds associated with different fundamental frequencies, reprinted with permission.[58] Copyright 2021, IOP Science. (F) Cylindrical model projections estimate modulation amplitude on electrode planes along the *Y* and *X* axes, including setups with rectangular electrodes in ratios of 1:1, 1:2, and 1:4, reprinted from ref 154. Available under a CC-BY 4.0. Copyright [2019] [IEEE].

frequencies allowing for more localized and precise effects. Static modulation, short-term stabilization of neural activity (e.g., γ oscillations), is relative to baseline levels without inducing lasting plasticity. This contrasts with dynamic modulation, which involves real-time, frequency-specific alterations in neuronal excitability (e.g., theta entrainment). The multiscale model evaluates how parameters such as membrane time constant (τ_m) and $GABA_b$ inhibition influence TI stimulation's sensitivity and selectivity across cortical and deep brain regions. By quantifying how these parameters govern transient stabilization (static) versus rapid excitability shifts (dynamic), the model enables precise tuning of TI protocols for targeted therapeutic outcomes such as transient oscillation stabilization in epilepsy or sustained plasticity in motor rehabilitation.

The spatial distribution of electric field magnitude and amplitude modulation along the posterior-anterior axis reveals how the electric field is distributed across deep brain structures and superficial cortical regions[93] (Figure 6E). This can confirm the effectiveness of TI in achieving targeted modulation of deep brain regions, such as the nucleus accumbens and putamen, while maintaining a minimal impact on cortical areas. By optimization of electrode placement and selection of the montage configuration, TI stimulation can achieve high precision, ensuring that deep brain regions are modulated effectively while avoiding unintended cortical stimulation.

Directional Specificity. The orientation of the electric field, whether applied along the mediolateral (ML) or anteroposterior (AP) axis determines the effectiveness of stimulation, especially for deep brain structures. ML stimulation typically uses symmetric electrode placements along the mediolateral axis (Table 3). This configuration creates lateral electric fields and is effective for enhancing interhemispheric communication and modulating motor pathways, making it ideal for regions such as the motor cortex and hippocampus. On the other hand, AP stimulation involves asymmetric electrode placements along the anterior-posterior axis, targeting long-range AP pathways. This configuration is effective for modulating the cingulate cortex and prefrontal cortex and is often used for applications involving executive functions, attention regulation, and spinal cord stimulation. The selection of electrode placement and orientation directly impacts the stimulation's depth, focality, and ability to selectively target desired brain regions.

The precision of TI stimulation is enhanced by considering the orientation of the electric field in relation to the target neuronal structures. Neuronal responsiveness to electric fields is anisotropic and varies based on the alignment of the electric field with the neurons' morphology, particularly the orientation

https://doi.org/10.1021/acsnano.5c15238
ACS Nano XXXX, XXX, XXX−XXX

of their dendrites and axons.[145] This is significant in the cortex, where neurons are often organized parallel to the cortical surface. A critical factor in optimizing TI stimulation is ensuring that the electric field is aligned to activate neurons efficiently. This alignment is achieved by strategically orienting the electrode configuration to maximize the effect on neurons in the target region while minimizing the influence on adjacent, off-target areas. Figure 7A illustrates the electric field generated by two orientations, with the maximum envelope placed at the same location in the hippocampus at the CA3-CA1 border.[59] Despite the maximum field strength being positioned similarly in both orientations, the direction of the electric field lines varies: in the ML orientation, the field is parallel to the axons of the hippocampus, whereas in the AP orientation, the field is perpendicular to these axons. The ML orientation, aligned with the long axis of the axons, enhances depolarization across a larger segment of the axonal membrane, making the stimulation more efficient[59,61] (Figure 7B). On the other hand, the AP orientation, which crosses a shorter segment of the axon, is less efficient for activating neurons. This demonstrates the importance of electrode orientation in optimizing TI stimulation's depth and precision. By aligning the electric field parallel to the axonal direction, TI stimulation lowers the threshold for inducing seizure-like activity, enhancing the capacitive coupling along the axons and promoting more effective neuronal activation. This effect is pronounced in the ML orientation, where the electric field is aligned with a long segment of the axonal membrane, which improves the depolarization process. The electric field achieves its maximal effect in the target brain region, while the off-target regions experience less focused modulation[145] (Figure 7C). This demonstrates the capability of TI stimulation to selectively influence neural activity in specific brain regions while minimizing unintended effects on surrounding areas.

Electrode Distance. Electrode distance in TI electrical stimulation is a crucial factor that directly influences the depth of stimulation within the brain. This relationship between electrode spacing and penetration depth can be described by a linear equation, enabling precise adjustments to the target depth based on electrode placement. The linear nature of this relationship allows for straightforward modulation of the stimulation depth, which is essential for targeted interventions in research and potential therapeutic applications[44,65,146] (Figure 8A,B). The depth d of the target area is linearly proportional to the distance s between the electrodes

$$d = k \times s \tag{4}$$

where k is a proportionality constant that depends on factors including tissue conductivity, electrode configuration, and stimulation frequency. This linearity allows for predictable modulation of target depth and provides a theoretical basis for designing stimulation montages. This linear relationship was validated through distributed electrode stimulation mapping (DESM) in invasive DBS modeling.[147] Using FEM simulations based on human brain anatomy, Collavini et al. demonstrated that increasing electrode spacing produced proportional increases in stimulation depth,[147] with k ranging from 0.42 to 0.51 depending on gray/white matter anisotropy. Although this study confirmed the linearity of electrode spacing effects, it was conducted in the context of invasive DBS leads and therefore does not fully capture the biophysical constraints of noninvasive TI, where current should traverse the scalp, skull, and cerebrospinal fluid before reaching neural tissue (Figure 8A,B). Complementary evidence supporting the linear model has emerged from experimental TI studies using noninvasive electrode configurations. In rodent models, scalp electrode spacing of ∼2.6 mm (placed at −0.55 mm and 2.05 mm mediolateral, −0.5 mm anteroposterior from bregma) generated a stimulation depth of ∼1.2 mm under low-intensity fields (<1 V m^{-1}), resulting in $k \approx 0.46$.[148] These data confirm that when stimulation intensities are below nonlinear neuronal response thresholds, electric field propagation behaves predictably and adheres to linear superposition principles. Extending these findings to human geometry, FEM simulations based on MRI-derived head models (n = 5) predict slightly lower k values (∼0.38 to 0.43), reflecting increased current attenuation across thicker skull and scalp tissues.[149,150] The brain can be approximated as a linear system in TI stimulation due to the relatively low-intensity electric fields used, typically below 1 V m^{-1}. Within this range of intensities (0.1−1 V m^{-1}), the distribution of the electric field follows a predictable linear pattern, which enables a direct relationship between electrode spacing and the depth of field penetration. However, the proportionality constant k differs depending on anatomical constraints and current pathways: larger k values in invasive DBS simulations reflect direct access to neural tissue, whereas smaller values in noninvasive TI account for extracranial current dissipation.

Current Amplitude and Ratio. The sensitivity of envelope amplitude to distance and amplitude ratios in TI stimulation underscores the necessity for precise manipulation of the location and size of the peak stimulation area.[45] This precision is crucial for effectively targeting specific neuronal populations in minimally invasive therapeutic applications. TI stimulation utilizes the precise manipulation of the mediolateral shift of the peak stimulation area by adjusting the amplitude ratio of two currents, I_2 and I_1, along the x-axis.[151] The amplitude of these currents and their ratio directly affect this lateral displacement of the stimulation focus[148] (Figure 8C). By adjustment of this ratio, the peak stimulation zone can be shifted laterally while maintaining stability along the y-axis (anteroposterior direction), enabling precise targeting without physical electrode repositioning.

Electric Field Intensity and Envelope Amplitude. In TI stimulation, a unique interaction occurs between two sinusoidal electric fields of slightly different frequencies. When these fields overlap, they produce an amplitude-modulated (AM) electric field, crucial for modulating neuronal activity.[60,65] The intensity of this field, measurable by its zero-to-peak value,[146] provides a measure of the maximum electric field strength at a specific spatial location. An essential factor is the modulation depth of the field's amplitude, $E_{AM}(r_n)$, reflected by the peak-to-peak value of its envelope. However, tissue conductivity gradients enhance the field penetration depth (Figure 3A), enabling deeper modulation (Figure 5G). This modulation depth, vital for stimulating neuronal tissue, depends on the proximity to the electrodes and the amplitude ratio of the interacting electric fields, I_2/I_1 (Figure 8D). At a 1:1 amplitude ratio, maximum modulation depth is achieved, indicating a broad stimulation area due to the synergistic enhancement of overlapping fields.[107] Deviating from this ratio shifts the envelope's peak toward the weaker field, showing an inverse relationship between stimulated area size and amplitude difference, with larger amplitudes focusing stimulation more locally. The envelope amplitude's decay with distance from the electrodes[58] (Figure 8D) reflects electro-

https://doi.org/10.1021/acsnano.5c15238
ACS Nano XXXX, XXX, XXX−XXX

magnetic field propagation,[57] decreasing in strength due to energy dispersion. This decay, shaped by the spatial properties of the individual fields and their relative phases, indicates a smaller envelope amplitude farther from the electrodes (eq 5). The envelope's shape, influenced by constructive and destructive interference patterns, minimizes off-target activation and side effects, as envelope amplitude peaks near the field interference region and decays with distance from electrodes.[109,152] The envelope amplitude decreases with distance from the electrodes, reaching the maximum amplitude close to the field interference. Additionally, a higher current amplitude results in a more confined stimulated area as the dominant high-intensity field narrows the constructive interference area, reducing the region of peak modulation depth.

Frequency. By superimposing two high-frequency electric fields at slightly different frequencies within the brain, a beat phenomenon occurs where the difference between these frequencies creates a modulation envelope in the low-frequency range. Typically, the frequencies of the high-frequency electric fields are chosen based on the characteristics of the target neural populations around 1−2 kHz with a Δf of 5 or 10 Hz in mouse studies.[58] Precise targeting of specific neural populations is achieved by adjusting f_1 and f_2 so that Δf falls within an optimal range for activating the target neurons without affecting surrounding non-targeted neuronal populations. This selective targeting is possible because different neural populations have varying activation thresholds for low-frequency stimulation. As frequency increases, the electric field strengths required to reach motor thresholds also increase[58] (Figure 8E), indicating that high frequencies necessitate higher intensities to achieve comparable levels of neuronal activation.

Multichannel TI, which uses multiple electrical channels for stimulation, typically reduces the stimulation intensity by an average of ∼28% compared to single-channel TI.[109] This reduction results from the ability to stimulate neurons at lower voltages to achieve the desired effects. Multichannel TI can cover a wider cortical area and requires less voltage for equivalent activation levels,[109] likely due to more effective constructive interference patterns from multiple channels, which need less energy to reach motor thresholds. The observation that motor thresholds increase with frequency can be linked to various biophysical factors. At higher frequencies, current penetration is limited by tissue capacitive reactance and electrode-tissue interface impedance.[153] Higher frequencies offer more precise spatial targeting due to their localized effects but may require higher intensities to reach the necessary depth, potentially increasing the risk of unintended side effects. Therefore, when selecting the frequency and deciding between multichannel or single-channel stimulation, it is essential to balance these choices with the therapeutic goals, prioritizing both effectiveness and safety. Further research into identifying optimal parameters for the motor cortex, hippocampus, and sensory areas, particularly focusing on low frequencies in the theta (4−8) and delta (1−4) Hz ranges, shows promise for cognitive enhancement and memory consolidation. Conversely, higher frequencies are being explored for their potential to modulate sensory processing and motor functions.

Voltage Intensity and Phase. Current-controlled stimulation ensures consistent electric field strength ($E = V/d$, where V stands for voltage, E represents the electric field intensity, and d is the distance between electrodes, the field intensity varies directly with the applied voltage and inversely with the distance between electrodes), accounting for variable electrode-tissue impedance.[45] By modulating the voltage, adjustments can be made to the electric field's strength to ensure targeted and efficient stimulation confined to specific brain regions.

Computational models in TI stimulation visualize electric field modulation within a spherical domain, projecting modulation amplitudes onto planes along the x and y axes across electrode arrays[154] (Figure 8F). These models assess the impacts of various electrode configurations with current amplitude ratios of 1:1, 1:2, and 1:4, influencing the magnitude of currents through electrode pairs and, consequently, the electric field distribution. The spatial arrangement of these ratios and electrode positions creates unique electric field distributions within the spherical model, demonstrating the combined effect of voltage intensity and electrode placement on the field's reach. Models using electric field strengths of 0.7, 1, and 1.2 V m^{-1} show that adjusting electrode spacing is critical for maintaining consistent field intensity, which is crucial for achieving desired penetration into deeper tissue. Effective TI stimulation involves the precise calculation of the electric field magnitude and the interaction between fields from paired electrodes. This interaction affects the net electric field intensity, which is computed as the vector sum of their interactions[88]

$$E_{net} = \sqrt{E_1^2 + E_2^2 - 2E_1E_2\cos(\Delta\phi)} \tag{5}$$

where E_1 and E_2 are the field intensities from each electrode pair and $\Delta\phi$ is the phase difference between their fields due to temporal interference. The phase relationship between these high-frequency signals is crucial in determining the patterns of constructive or destructive interference within the target area and, thus, the shape of the resultant low-frequency modulation envelope. The magnitude of the electric field at any given point is determined by the vector sum of the fields from each electrode. When these fields overlap, their amplitudes combine, creating regions of high and low intensity based on their phase relationship. Constructive interference, indicated by a positive $\cos(\Delta\phi)$, occurs when the fields are in phase, resulting in a higher overall field magnitude. Conversely, a negative $\cos(\Delta\phi)$ when the fields are out of phase signifies destructive interference, reducing the field intensity. Accurate phase alignment is essential for maximizing modulation depth within the targeted neuronal population while minimizing stimulation of surrounding tissues. By adjusting these parameters, including electrode placement and frequencies, the field's depth and focus can be tailored to create a low-frequency modulation envelope that accurately targets therapeutic areas in deep brain regions while avoiding non-targeted regions.

Parameter Algorithms Optimization. The efficiency of TI stimulation hinges on the precise adjustment of the stimulation's depth and area of activation. This precision was generally achieved through trial-and-error or basic computational models,[155] adjusting the sum and ratio of currents via electrode pairs. Artificial neural networks (ANNs) offer a systematic method for determining optimal stimulation parameters, enhancing the process's accuracy and efficiency.[10,53] The efficiency of TI stimulation hinges on precise adjustment of the stimulation's depth and activation area. Historically, this precision relied on trial-and-error or basic computational models, adjusting current sums and ratios across electrode pairs.[155] ANNs offer a systematic approach to

https://doi.org/10.1021/acsnano.5c15238
ACS Nano XXXX, XXX, XXX−XXX

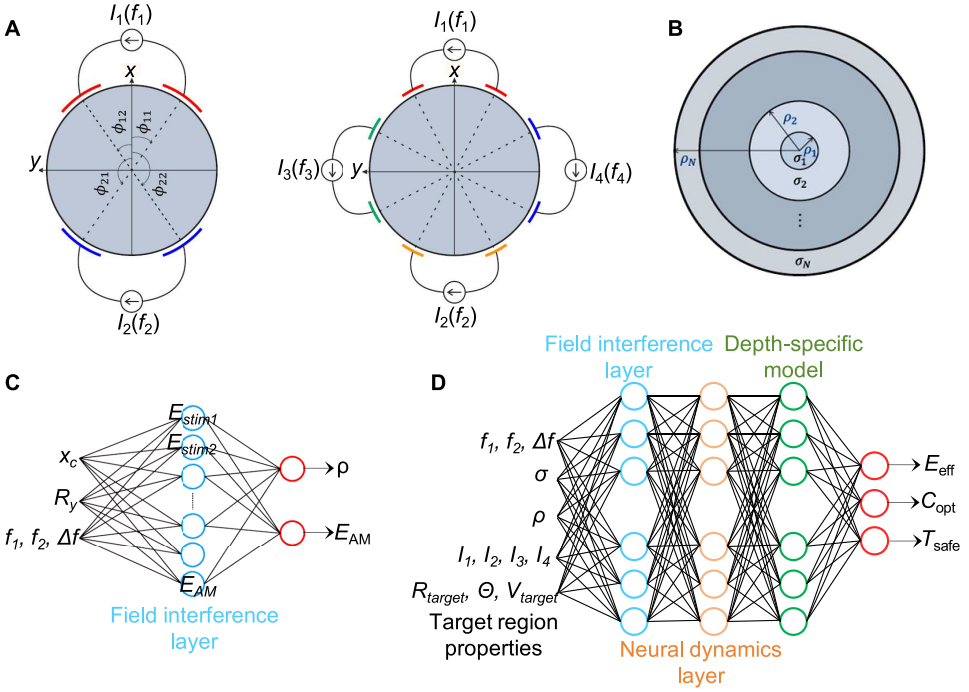

Figure 9. Artificial neural network (ANN) model for TI stimulation optimization. (A) Infinite homogeneous cylinder (IHC) model with two and four electrode pairs and (B) infinite inhomogeneous cylinder (IIC) model including tissue heterogeneity. The electric fields E_1 and E_2 generated by two electrode pairs at frequencies f_1 and f_2, respectively, interfere to produce a low-frequency modulation, represented by the envelope E_{AM}, which controls neural activation. φ, angles control the placement of electrodes around the cylindrical brain model. φ_{11} and φ_{12} are the angles for the first electrode pair; φ_{21} and φ_{22} are the angles for the second electrode pair. ρ_N, the outermost radius, represents the boundary of the tissue, σ is the conductivity, and ρ is the resistivity of the tissue, influencing the distribution of electric fields in the brain. R_x, R_y: Euclidean distances between the center of gravity and specific points within the brain-activated area, quantifying the location and size of the activated area in relation to the electrode configuration. Reprinted with permission.[107] Copyright 2019, IOP Science. (C) Single-layer and (D) multilayer ANN model to optimize the TI stimulation parameters. The network is structured with an input layer that incorporates various stimulation and tissue parameters, followed by a hidden layer where field interactions and neuronal responses are computed. The output layer predicts the efficiency of stimulation and neural activation, such as the electric field strength and neuromodulator effects. E_{stim1}, E_{stim2}: Electric fields generated by each electrode pair at the corresponding frequencies. E_{AM}: Amplitude modulation envelope, which governs the overall time-dependent variation in the electric field strength. Region-specific properties: R_{target}, target region conductivity; V_{target}, target region volume; Θ, orientation. Output layer predictions: E_{eff}, activation efficiency to activate neurons, accounting for the depth and focality of stimulation; T_{safe}, safety thresholds, which represent the limits of stimulation parameters to avoid undesired effects (tissue heating, excessive current density); C_{opt}, optimal combination of frequencies, currents, and electrode placements.

optimizing stimulation parameters, enhancing accuracy and efficiency by addressing the inverse problem identifying parameters to target specific neural regions.[10,53,156]

ANNs excel at correlating the stimulation area's center of gravity with input currents, enabling fine manipulation of field shape and position.[107] While dual-electrode setups limit focus through current symmetry, quad-electrode configurations independently adjust field distribution variables (R_x, R_y), improving precision.[45] These networks leverage simplified brain models (e.g., infinite homogeneous cylinder, IHC) to predict optimal parameters like current sum/ratio (Figure 9A), with inhomogeneous cylinder (IIC) models incorporating tissue heterogeneity to refine accuracy[107] (Figure 9B). Multilayer ANNs process inputs such as electric field strength, frequency, tissue conductivity, and electrophysiological properties (membrane resistance and ion channel density) to simulate neural responses (Figure 9C,D). Their output layers predict activation efficiency, safety thresholds, and optimal electrode placements, balancing therapeutic efficacy and off-target effects.[107]

Beyond ANNs, other machine learning paradigms provide complementary capabilities for optimizing TI neuromodulation. Convolutional neural networks (CNNs) enhance electrode placement by extracting spatial features from MRI and CT imaging, improving focus in individualized head models.[157−160] Recurrent architectures such as RNNs and LSTMs incorporate temporal dynamics, enabling prediction of neural responses to varying stimulation phases and frequencies.[10] Reinforcement learning has also emerged as a powerful strategy for adaptive stimulation, using real-time neural feedback to iteratively adjust parameters and maximize therapeutic efficacy.[161]

Despite these advances, ANN-based optimization still faces barriers to clinical translation. A primary challenge lies in the dependence on the data quality and diversity. Because ANN predictions are strongly shaped by training data, models trained on limited anatomical variability often fail in atypical anatomies. Internal validation studies demonstrate that targeting error increases by 18% when ANNs are applied to MRI data sets from patients with more than 10% hippocampal atrophy, compared to age-matched healthy controls. These errors disproportionately affect under-represented populations such as pediatric patients or individuals with neurodegenerative disease. Incorporating multiethnic, multiage cohorts and augmenting rare scenarios using generative adversarial networks (GANs) may significantly improve generalizability.[162]

https://doi.org/10.1021/acsnano.5c15238
ACS Nano XXXX, XXX, XXX−XXX

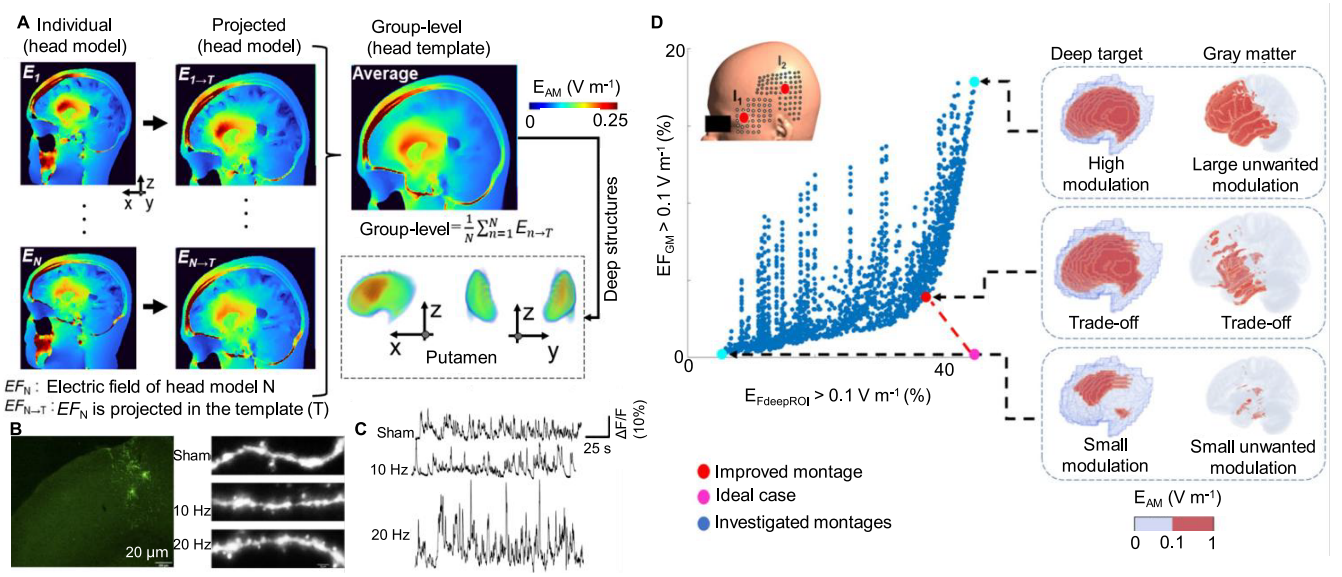

Figure 10. TI trials for deep brain stimulation. (A) Normalization of the electric field (EF) from an individual brain model (subject *N*, EF_N) to a common brain template ($EF_N \rightarrow T$). The group-level data represent the average of electric fields normalized to the template. Reprinted with permission.[78] Copyright 2024, Springer Nature. (B) TI stimulation increased dendritic spine density in M1 neurons. (C) Representative calcium signal traces ($\Delta F/F$) of M1 neurons during treadmill running. Sham represents no stimulation. TI stimulation with Δf of 10 and 20 Hz frequencies can observe the impact on dendritic spine density. (B, C) Reprinted with permission.[64] Copyright 2024, Springer. (D) The trade-off between neuromodulation volume in the deep brain target and gray matter (unwanted modulation), reprinted with permission.[78] Copyright 2024, Springer Nature.

When integrating ANNs to optimize TI stimulation parameters, design of network architecture including the number of neurons and layers is essential to ensure accurate predictions and prevent overfitting, which would impair generalization to new data.[163] Implementing cross-validation methods like k-fold is critical to ascertain the model's ability to generalize and maintain reliability across different data sets.[164] Moreover, generalization to an unseen anatomy presents an additional limitation. ANNs often fail in edge cases involving structural abnormalities, such as skull defects or intracranial tumors that alter current flow. An ANN model misestimated TI field distributions with meningiomas was reported to target errors up to 2.3 mm.[165] Recent efforts address this by integrating physics-informed corrections based on FEM simulations, yielding hybrid models that better handle anomalous conductivity landscapes.[166]

Algorithmic optimization accelerates TI precision, expanding therapeutic possibilities for neurological disorders. However, ANN utility depends on addressing data biases, generalizability, and interpretability, challenges requiring interdisciplinary collaboration among engineers, radiologists, and regulators. By integrating diverse anatomical data, hybrid physics-ANN models, and explainable AI tools, these limitations can be mitigated, unlocking TI's potential for targeted neuromodulation. While ANNs accelerate TI optimization, their utility remains contingent on addressing data biases and interpretability gaps, challenges that demand interdisciplinary collaboration between engineers, radiologists, and regulatory bodies.

TI TRIALS FOR DEEP BRAIN STIMULATION

TI stimulation offers the potential to precisely modulate deep brain regions with a minimal impact on surrounding tissues. By leveraging the interference of high-frequency electric fields, TI allows for selective neuromodulation at different depths of the brain, which makes it a promising therapeutic tool for treating various neurological conditions including epilepsy, cognitive disorders, and motor dysfunctions. The efficacy of TI stimulation depends on a clear understanding of how electric fields distribute across different brain structures. The electric fields from individual brain models were normalized to a common brain template using the subject2mni function in SimNIBS[78] (Figure 10A). This enables comparison of electric field distributions across subjects from diverse populations including healthy individuals, the elderly, and stroke patients. By aligning individual data with the template, researchers can calculate the average electric field across a population, facilitating group-level analysis. This normalization method provides valuable insights into how TI stimulation influences brain activity in different demographic groups and can help guide personalized treatment plans for conditions such as stroke recovery and age-related cognitive decline. TI stimulation can lead to significant changes in dendritic spine density in the primary M1 motor cortex[64] (Figure 10B). Dendritic spines were imaged using sparsely labeled neurons before and after 7 days of TI stimulation, with both the M-10 Hz and M-20 Hz groups showing a significant increase in spine density compared to the M-Sham group, suggesting that TI stimulation enhances synaptic plasticity.

The impact of TI stimulation on neuronal activity is shown through calcium signal traces from M1 neurons during a treadmill running task[64] (Figure 10C). GCaMP fluorescence was used to monitor the dynamic activity of neurons in response to TI stimulation. TI stimulation can enhance neuronal activity compared to the sham group. Figure 10D shows the neuromodulation volume and its relationship with both the gray matter and deep brain regions.[78] The neuromodulation volume was measured by calculating the regions where the electric field exceeded a certain neuromodulation threshold (0.1 V m^{-1}). A trade-off exists between

https://doi.org/10.1021/acsnano.5c15238
ACS Nano XXXX, XXX, XXX−XXX

neuromodulation in the superficial gray matter and deeper brain structures such as the putamen, caudate nucleus, and hippocampus. This balance is crucial for optimizing TI stimulation for deep brain targets, such as those involved in epilepsy treatment, cognitive enhancement, and spinal cord stimulation. Through analysis of electric field distributions, calcium signaling, and dendritic spine density, TI stimulation has been demonstrated to enhance synaptic plasticity, motor performance, and cognitive function. The optimization of stimulation parameters through group-level normalization ensures that neuromodulation is effective and focal. By further refining electrode placements and understanding the neuromodulation volume, TI stimulation can be tailored for therapeutic applications, providing a promising tool for the noninvasive treatment of epilepsy, stroke recovery, and motor impairments.

CHALLENGES

Complex Interactions and Conduction Block. Unlike FUS, which relies on acoustic energy deposition and requires MR thermography to monitor thermal risks,[31] tTIS operates at intensities (<1 V m^{-1}) well below thresholds for tissue heating. Computational models[48] and empirical measurements[167] confirm that TI induces negligible temperature rise (ΔT < 0.1 °C), eliminating the need for thermal monitoring. However, achieving therapeutic efficacy in deep brain targets (e.g., hippocampus, striatum) necessitates millimeter-level precision in electrode placement to ensure constructive interference at the target site. Even minor misalignments (>2 mm) can shift the modulation envelope to off-target regions, undermining therapeutic outcomes. In clinical settings, suprathreshold TI intensities capable of inducing conduction blocks to inhibit neural activity are infeasible in humans due to safety risks.[46,49,92,150] Critically, human tTIS adheres to strict safety margins, with stimulation intensities capped below 2 mA to prevent discomfort and tissue damage, as suprathreshold protocols risk exceeding cutaneous pain thresholds.[68,167] While higher currents improve penetration depth, they risk exceeding pain thresholds, creating a trade-off between efficacy and tolerability. Current methodologies, reliant on markers like c-fos to assess neural activation, predominantly capture somatic activity and fail to detect axonal conduction blocks or subthreshold network effects.[39,80] Critically, human trials remain limited in the sample size and long-term outcomes. A recent study targeting the subthalamic nucleus in Parkinson's disease demonstrated short-term tremor reduction but lacked longitudinal follow-up.[66] To address these gaps, geometric 3D electrode mapping[111,130] and closed-loop algorithms[168] are being developed to refine targeting while maintaining safe thresholds. These advancements, combined with pharmacological adjuncts, aim to enhance specificity while minimizing off-target inhibition.

Asymmetry and Signal Manipulation. Experiments involving asymmetric envelopes where depolarizing and hyperpolarizing peaks are manipulated demonstrate neurons' preference for cathodal components, lending credence to the integrator mechanism over the envelope extraction theory.[89] Furthermore, amplitude steering, which involves adjusting the amplitude of one signal relative to another, shifts activation regions toward the stronger field, contradicting predictions based solely on envelope amplitude.[49,169,170] This asymmetry complicates targeting but enables the directional control of neuromodulation. Increasing the amplitude of the posterior electrode pair can shift stimulation focus anteriorly within the hippocampus, bypassing cortical regions.[49] Achieving consistent inhibitory neuromodulation requires precise control of the TI parameters. Overstimulation risks unintended excitation, while subthreshold amplitudes may fail to suppress pathological activity.[167]

Data Processing and Error Management. TI poses unique data processing challenges, particularly in distinguishing target engagement from artifactual signals. Electromyography (EMG) and electroencephalography (EEG) require adaptive filtering to isolate neural responses from stimulation artifacts.[171,172] Electrode displacement or impedance changes due to tissue dehydration can distort the recruitment curves, leading to inaccurate threshold estimations. To mitigate drift, real-time error detection systems using Kalman filtering and machine learning are under development.[173] These tools dynamically adjust stimulation parameters based on feedback, improving reliability in heterogeneous patient populations.

CONCLUSION

TI Stimulation Specificity and Risks of Unintended Modulation in Adjacent Regions. The depth-specific targeting achievable with TI stimulation, enabled by constructive interference of high-frequency electric fields, represents a shift in noninvasive neuromodulation. Unlike conventional techniques, TI can selectively recruit deep neural structures by exploiting tissue conductivity gradients and the nonlinear dynamics of voltage-gated ion channels. These mechanisms allow subthreshold oscillatory fields to summate into action potential, generating depolarizations at depth while largely sparing the overlying cortex. Nevertheless, unintended modulation of adjacent regions remains a critical and unresolved challenge, particularly when targeting small or anatomically complex nuclei such as the STN or amygdala, where millimeter-scale precision is required.

Field spread arises primarily from heterogeneity in tissue conductivity and limitations of electrode configurations. At interfaces such as gray–white matter boundaries or cerebrospinal fluid compartments, electric fields may be refracted or scattered, producing diffusion of stimulation effects beyond the intended focal zone. Finite element simulations in realistic human head models indicate that attempts to target the nucleus accumbens can inadvertently deliver 15–20% of the target field strength to the adjacent globus pallidus externus *via* preferential conduction along white matter tracts. Similarly, the conventional 2–3 electrode montages often used in early TI studies generate relatively broad interference patterns; in rodent hippocampal stimulation experiments, this has been associated with measurable c-Fos expression in the entorhinal cortex, demonstrating the physiological engagement of off-target circuits even in the absence of overt behavioral effects.

These field-spread effects are not merely technical nuisances but carry potential functional risks. During STN targeting in Parkinson's disease, unintentional activation of fibers within the internal capsule could precipitate dyskinesia or motor discomfort. To address this limitation, a multimodal mitigation strategy is required. One promising direction is the use of adaptive electrode arrays comprising 4–6 independently controlled channels. Optimization of interference patterns using machine learning algorithms trained on large MRI data sets has already reduced off-target field intensity by more than 40% in simulation studies. Complementing hardware innova-

https://doi.org/10.1021/acsnano.5c15238
ACS Nano XXXX, XXX, XXX–XXX

tion, patient-specific finite element modeling based on individual MRI or CT improves prediction of field propagation and reduces targeting error by approximately 35% compared to generic anatomical models in preliminary epilepsy studies. Finally, the integration of real-time neurophysiological feedback offers a dynamic safeguard against unintended stimulation. Ultrafast fMRI or high-density EEG can monitor neural activation during TI delivery and trigger rapid parameter adjustments when off-target responses exceed predefined thresholds, a strategy that reduced seizure duration by 76% in rodent epilepsy models using EEG-triggered TI modulation. These developments suggest that while field spread remains a challenge, it is increasingly tractable through the convergence of computational modeling, adaptive stimulation technologies, and closed-loop feedback control.

Safety Considerations for Long-Term Exposure to TI Fields. Although the low-intensity electric fields used in TI stimulation (typically $\leq$ 1.5 mA) avoid significant tissue heating, this is a clear advantage over energy-intensive modalities such as focused ultrasound. Current evidence suggests that thermal effects are minimal; even under conservative assumptions of daily 1 h stimulation over a 12-month period, modeled temperature increases in deep brain regions do not exceed 0.8 °C, well below the 4 °C threshold associated with protein denaturation.[49,92,150] Nonetheless, continuous monitoring is prudent. Adaptive power modulation incorporating real-time scalp thermometry and intermittent pulsed stimulation protocols (e.g., 10 min on, 5 min off) offers effective safeguards against cumulative thermal load.

More complex are the neurophysiological risks associated with chronic subthreshold polarization. Prolonged modulation of membrane potentials may lead to homeostatic down-regulation of voltage-gated ion channels or maladaptive reorganization of oscillatory networks. Experimental countermeasures are emerging: dynamic frequency tuning, in which modulation frequencies alternate between 10 and 15 Hz, has preserved response efficacy in vitro while minimizing neural desensitization. Longitudinal studies in nonhuman primates further provide continuous EEG surveillance to detect early epileptiform tendencies, thus enabling timely adjustment of stimulation parameters.

Another concern relates to neurovascular safety. While short-term TI exposure has not been shown to compromise blood–brain barrier integrity, the consequences of chronic delivery remain uncertain. Early rodent studies extending over two years are now combining dynamic contrast-enhanced MRI with cerebrospinal fluid cytokine profiling to detect subtle blood–brain barrier perturbations or microglial activation that may signal low-grade neuroinflammation. Finally, safety considerations should account for vulnerable populations. Both pediatric and geriatric brains exhibit heightened susceptibility to neuromodulatory interventions due to ongoing neurodevelopmental processes or an age-related decline in homeostatic resilience. Accordingly, age-stratified preclinical studies using juvenile and aged rodent cohorts combined with Bayesian dose–response modeling are now being used to refine population-specific safety thresholds.

Computational and Hardware Advancements to Optimize TI Stimulation. The successful translation of TI stimulation into clinical practice depends on coordinated advances in both computational modeling and hardware engineering to improve targeting precision, usability, and long-term patient adherence. Recent developments in computational neuroscience are enabling personalization. Multiple electrode pairs can be adopted to achieve focused targeting of brain regions, enhancing specificity and reducing nontarget effects. Additionally, genetic algorithms and gradient descent methods iteratively adjust stimulation parameters by evaluating numerous configurations to determine the most effective setup for precise neuromodulation. FEA and machine learning models predict electric field distributions within the brain, accounting for anatomical complexity and tissue conductivity variations. These models identify optimal current injections and electrode configurations to maximize delivery to targets such as the hippocampus or basal ganglia. Meanwhile, real-time neural response monitoring enables dynamic parameter adjustments, improving accuracy.

Patient-specific multiphysics models that integrate high-resolution electromagnetic field simulations with Hodgkin–Huxley neuronal dynamics can now predict the spatial distribution of action potential initiation with submillimeter precision (<0.5 mm). This capability has already demonstrated selective activation of hippocampal CA3 subfields while sparing adjacent dentate gyrus circuits in simulation studies, highlighting the feasibility of fine-grained targeting of deep structures. These models are being complemented by adaptive control strategies: deep learning-based closed-loop systems capable of jointly analyzing EEG and fMRI signals, classifying ongoing neural responses as therapeutic or adverse, and dynamically adjusting stimulation parameters. These AI-driven controllers reduce the total stimulation time by up to 40% in large-scale in silico trials by using Bayesian optimization to converge rapidly on effective dosing strategies.

Parallel innovation in hardware design is transforming TI delivery systems from laboratory prototypes into clinically viable platforms. Flexible, conformal electrode arrays manufactured from MRI-compatible polyimide films incorporate embedded temperature and impedance sensors, which mitigate scalp irritation by ∼45% compared with conventional rigid electrodes, while improving the homogeneity of current distribution across the scalp. Miniaturized, wearable TI stimulators based on custom application-specific integrated circuits (ASICs) now weigh less than 50 g and provide more than 24 h continuous operation, enabling ambulatory neuromodulation without compromising performance. Human fMRI studies have confirmed that these portable systems achieve hippocampal activation patterns comparable to those produced by benchtop stimulators. Meanwhile, increases in channel density enhance spatial precision. High-density platforms offering 16 to 32 independently controlled current channels with 0.1 mA resolution can sculpt interference fields with substantially greater focality, reducing off-target modulation by up to 55% when stimulating small or anatomically complex targets such as the amygdala. Emerging modalities such as magnetic TI stimulation (TI-MS) offer alternative approaches. TI-MS uses interfering kHz-frequency magnetic fields to induce low-frequency electric currents, bypassing electrode contact issues inherent to electrical methods.[174] While promising, its spatial resolution and depth penetration remain under exploration.[175] These computational and engineering advances lay the foundation for safe, precise, and patient-centered TI neuromodulation therapies.

Integration with Imaging Modalities (fMRI, EEG) for Closed-Loop Neuromodulation. Closed-loop TI systems that integrate functional MRI and high-density EEG offer a powerful solution to the long-standing trade-off between

https://doi.org/10.1021/acsnano.5c15238
ACS Nano XXXX, XXX, XXX–XXX

spatial and temporal precision in neuromodulation. Real-time fMRI integration provides anatomical and network-level guidance during stimulation: ultrafast echo-planar imaging sequences can detect BOLD signal fluctuations within several seconds, enabling rapid verification of engagement of deep brain targets. In proof-of-concept studies, such real-time monitoring reduced the unintended activation of adjacent structures during STN stimulation from 18 to 4% in healthy participants. Beyond focal targeting, resting-state connectivity maps derived from fMRI also allow TI stimulation to be directed toward pathological network hubs rather than single nuclei. In major depressive disorder, targeting the posterior cingulate cortex to modulate the default mode network resulted in more than a 2-fold improvement in anhedonia compared with conventional nucleus-specific stimulation strategies.

EEG contributes complementary capabilities by providing millisecond-scale feedback on neural dynamics. High-density EEG combined with source localization enables the rapid detection of pathological activity and near-instantaneous stimulation adjustments. In rodent epilepsy models, this framework allowed TI delivery to be triggered within 200 ms of interictal spike onset, reducing the seizure duration by 76%. Similarly, in Parkinson's disease, synchronizing the low-frequency TI envelope with endogenous β-band oscillations (13−30 Hz) improved motor outcomes by 41% over nonphase-locked stimulation. The synergistic use of fMRI and EEG in a unified closed-loop design is therefore emerging as the gold standard for precision neuromodulation.[6,176] In Parkinson's disease, prestimulation fMRI enables accurate localization of the STN, EEG continuously monitors β oscillatory biomarkers during TI delivery, and poststimulation fMRI confirms focal target engagement while verifying the absence of unintended activation in sensitive fiber tracts such as those in the internal capsule. This multimodal integration not only enhances both targeting accuracy and safety but also enables adaptive, patient-specific neuromodulation tailored to evolving brain states in real time.

Priority Targets and Barriers for Clinical Translation. TI stimulation occupies a unique position in the neuromodulation landscape by enabling noninvasive access to deep neural circuits that are central to neurological and psychiatric disorders yet largely unreachable by existing technologies. Prioritization of clinical indications can be guided by the mechanistic fit, severity of unmet need, and strength of preclinical evidence. Based on these criteria, Parkinson's disease emerges as a leading target: stimulation of the STN *via* TI has reduced akinesia by 65% in rodent models, and nearly 40% of patients with Parkinson's disease are ineligible for DBS due to surgical risk or comorbidity, underscoring a substantial therapeutic gap. Refractory epilepsy represents a compelling early indication. TI targeting of hippocampal circuits has suppressed epileptiform discharges in ex vivo human tissue, and with 30% of patients resistant to pharmacotherapy, TI may offer a nonsurgical alternative to resection or responsive neurostimulation. Major depressive disorder is another high-priority application, where TI directed at monoaminergic hubs such as the dorsal raphe nucleus (DRN) or nucleus accumbens (NAc) has demonstrated mechanistic validity; DRN-TI increases hippocampal serotonin release by 28% in rodent studies, while NAc-TI modulates dopaminergic signaling relevant to motivational circuitry.

Despite this promise, successful clinical translation requires overcoming the barriers in regulation, technology, and ethics. Regulatory uncertainty remains a central challenge, as current frameworks lack clear guidance for noninvasive technologies capable of deep brain stimulation. A pragmatic path forward is to pursue hybrid Phase 0/1 trial designs that combine cadaveric validation of targeting accuracy with small-scale safety studies in ∼ 20 patients while engaging regulatory agencies early to define least-burdensome data requirements. Technical variability poses a second challenge: interindividual differences in skull conductivity, cortical atrophy, and brain morphology can reduce targeting precision by more than 20% if uncorrected. Real-time adaptive TI guided by MRI-based field estimation and longitudinal primate data on neuronal excitability stability over 12 months can mitigate this variability.

In sum, TI stimulation represents an avenue for noninvasive deep brain modulation, with potential to revolutionize treatment for Parkinson's disease, epilepsy, and depression. Addressing the challenges of field spread, long-term safety, and clinical translation requires interdisciplinary collaboration across engineering, neuroimaging, and regulatory science. By integrating adaptive technologies, closed-loop imaging feedback, and patient-specific modeling, TI can bridge the gap between preclinical promise and clinical impact, complementing existing modalities such as FUS and TMS to advance precision neuromodulation.

AUTHOR INFORMATION

Corresponding Authors

Guosong Hong − *Department of Materials Science and Engineering, Stanford University, Stanford, California 94305, United States; Wu Tsai Neurosciences Institute, Stanford University, Stanford, California 94305, United States;* orcid.org/0000-0002-8858-4471; Email: guosongh@stanford.edu

[⊥]**Jun Chen** − *Department of Bioengineering, University of California, Los Angeles, Los Angeles, California 90095, United States;* orcid.org/0000-0002-3439-0495; Email: jun.chen@ucla.edu

Authors

Shumao Xu − *Department of Bioengineering, University of California, Los Angeles, Los Angeles, California 90095, United States;* orcid.org/0000-0003-2062-0226

Han Cui − *Department of Materials Science and Engineering, Stanford University, Stanford, California 94305, United States; Wu Tsai Neurosciences Institute, Stanford University, Stanford, California 94305, United States;* orcid.org/0000-0001-6473-9232

Xiao Xiao − *Department of Bioengineering, University of California, Los Angeles, Los Angeles, California 90095, United States;* orcid.org/0000-0002-7861-5596

Farid Manshaii − *Department of Bioengineering, University of California, Los Angeles, Los Angeles, California 90095, United States*

Complete contact information is available at: https://pubs.acs.org/10.1021/acsnano.5c15238

Author Contributions

[‖]S.X. and H.C. contributed equally.

Notes

The authors declare no competing financial interest.

https://doi.org/10.1021/acsnano.5c15238
ACS Nano XXXX, XXX, XXX−XXX

[⊥]Lead contact.

ACKNOWLEDGMENTS

J.C. acknowledges the Vernroy Makoto Watanabe Excellence in Research Award at the UCLA Samueli School of Engineering, the Office of Naval Research Young Investigator Award (Award ID: N00014-24-1-2065), NIH Grant (Award ID: R01 CA287326 and R01 HL175135), the American Heart Association Innovative Project Award (Award ID: 23IPA1054908), the American Heart Association Transformational Project Award (Award ID: 23TPA1141360), the American Heart Association's Second Century Early Faculty Independence Award (Award ID: 23SCEFIA1157587), and the Brain & Behavior Research Foundation Young Investigator Grant (Grant Number:30944). G.H. acknowledges support from an NSF CAREER award (2045120), a Scholars Award from the Rita Allen Foundation, funding from FUS Foundation, donations from the Spinal Muscular Atrophy (SMA) Foundation and the Pinetops Foundation, as well as seed funding from both the Wu Tsai Neurosciences Institute and the Bio-X Initiative at Stanford University. Additionally, this work was supported by the National Science Foundation under grant number 1828993, the National Science Foundation Graduate Research Fellowship Program under grant number DGE-1656518, and the NIH Stanford Graduate Training Program in Biotechnology under award number T32GM141819. The views expressed in this material are solely those of the authors and do not necessarily represent the views of the National Science Foundation. H.C. acknowledges support from a Stanford Interdisciplinary Graduate Fellowship as the David L. Sze and Kathleen Donohue Interdisciplinary Fellow.

REFERENCES

(1) Fasano, A.; Aquino, C. C.; Krauss, J. K.; Honey, C. R.; Bloem, B. R. Axial disability and deep brain stimulation in patients with Parkinson disease. *Nat. Rev. Neurol.* **2015**, *11*, 98−110.
(2) Limousin, P.; Foltynie, T. Long-term outcomes of deep brain stimulation in Parkinson disease. *Nat. Rev. Neurol.* **2019**, *15*, 234−242.
(3) Scangos, K. W.; State, M. W.; Miller, A. H.; Baker, J. T.; Williams, L. M. New and emerging approaches to treat psychiatric disorders. *Nat. Med.* **2023**, *29*, 317−333.
(4) Xu, S.; Scott, K.; Manshaii, F.; Chen, J. Heart-brain connection: How can heartbeats shape our minds? *Matter* **2024**, *7*, 1684−1687.
(5) Sheth, S. A.; Mayberg, H. S. Deep Brain Stimulation for Obsessive-Compulsive Disorder and Depression. *Annu. Rev. Neurosci.* **2023**, *46*, 341−358.
(6) Chen, S.; Xu, S.; Fan, X.; Xiao, X.; Duan, Z.; Zhao, X.; Chen, G.; Zhou, Y.; Chen, J. Advances in 2D materials for wearable biomonitoring. *Mater. Sci. Eng. R* **2025**, *164*, No. 100971.
(7) Xu, S.; Ge, M.; Chen, S.; Wang, Y.; Tang, Y.; Wang, J.; Cui, X.; Sun, C.; Zeng, H.; Wang, N.; et al. Leveraging Laser-Patterned Copper Electrodes for Personal Healthcare. *Small Methods* **2025**, *35*, No. e00056.
(8) Zhao, D.; Huang, R.; Gan, J.-M.; Shen, Q.-D. Photoactive nanomaterials for wireless neural biomimetics, stimulation, and regeneration. *ACS Nano* **2022**, *16*, 19892−19912.
(9) Wang, Y.; Yang, Z.; Wang, J.; Ge, M.; Wang, N.; Xu, S. Brain-Body Interactions in Ischemic Stroke: VNS Reprograms Microglia and FNS Enhances Cerebellar Neuroprotection. *Stroke* **2025**, *56*, e267−e278.
(10) Xu, S.; Liu, Y.; Lee, H.; Li, W. Neural interfaces: Bridging the brain to the world beyond healthcare. *Exploration* **2024**, *4*, No. 20230146.
(11) Xu, S.; Chen, G.; Scott, K.; Manshaii, F.; Chen, J. Soft electrochemical actuators for intraoperative nerve activity monitoring. *Matter* **2024**, *7*, 2795−2797.
(12) Chen, R.; Canales, A.; Anikeeva, P. Neural recording and modulation technologies. *Nat. Rev. Mater.* **2017**, *2*, 16093.
(13) Won, S. M.; Song, E.; Reeder, J. T.; Rogers, J. A. Emerging modalities and implantable technologies for neuromodulation. *Cell* **2020**, *181*, 115−135.
(14) Wiseman, M.; Sewell, I. J.; Nestor, S. M.; Giacobbe, P.; Hamani, C.; Lipsman, N.; Rabin, J. S. Cognitive effects of focal neuromodulation in neurological and psychiatric disorders. *Nat. Rev. Psychol.* **2024**, *3*, 242−260.
(15) Shen, K.; Chen, O.; Edmunds, J. L.; Piech, D. K.; Maharbiz, M. M. Translational opportunities and challenges of invasive electrodes for neural interfaces. *Nat. Biomed. Eng.* **2023**, *7*, 424−442.
(16) Hong, G.; Lieber, C. M. Novel electrode technologies for neural recordings. *Nat. Rev. Neurosci.* **2019**, *20*, 330−345.
(17) Dai, X.; Hong, G.; Gao, T.; Lieber, C. M. Mesh nanoelectronics: seamless integration of electronics with tissues. *Acc. Chem. Res.* **2018**, *51*, 309−318.
(18) Woods, G. A.; Rommelfanger, N. J.; Hong, G. Bioinspired materials for in vivo bioelectronic neural interfaces. *Matter* **2020**, *3*, 1087−1113.
(19) Chen, Y.; Wang, S.; Zhang, F. Near-infrared luminescence high-contrast in vivo biomedical imaging. *Nat. Rev. Bioeng.* **2023**, *1*, 60−78.
(20) Su, Y.; Walker, J. R.; Hall, M. P.; Klein, M. A.; Wu, X.; Encell, L. P.; Casey, K. M.; Liu, L. X.; Hong, G.; Lin, M. Z.; Kirkland, T. A. An optimized bioluminescent substrate for non-invasive imaging in the brain. *Nat. Chem. Biol.* **2023**, *19*, 731−739.
(21) Schmidt, E. L.; Ou, Z.; Ximendes, E.; Cui, H.; Keck, C. H.; Jaque, D.; Hong, G. Near-infrared II fluorescence imaging. *Nat. Rev. Methods Primers* **2024**, *4*, 23.
(22) Cui, H.; Zhao, S.; Hong, G. Wireless deep-brain neuromodulation using photovoltaics in the second near-infrared spectrum. *Device* **2023**, *1*, No. 100113.
(23) Xu, S.; Manshaii, F.; Chen, J. Is Deep Brain Imaging on the Brink of Transformation with a Bioluminescence Molecule? *BMEMat* **2024**, *2*, No. e12115.
(24) Lozano, A. M.; Lipsman, N.; Bergman, H.; Brown, P.; Chabardes, S.; Chang, J. W.; Matthews, K.; McIntyre, C. C.; Schlaepfer, T. E.; Schulder, M.; et al. Deep brain stimulation: current challenges and future directions. *Nat. Rev. Neurol.* **2019**, *15*, 148−160.
(25) Krauss, J. K.; Lipsman, N.; Aziz, T.; Boutet, A.; Brown, P.; Chang, J. W.; Davidson, B.; Grill, W. M.; Hariz, M. I.; Horn, A.; et al. Technology of deep brain stimulation: current status and future directions. *Nat. Rev. Neurol.* **2021**, *17*, 75−87.
(26) Sheth, S. A.; Mayberg, H. S. Deep brain stimulation for obsessive-compulsive disorder and depression. *Annu. Rev. Neurosci.* **2023**, *46*, 341−358.
(27) Holtzheimer, P. E.; Husain, M. M.; Lisanby, S. H.; Taylor, S. F.; Whitworth, L. A.; McClintock, S.; Slavin, K. V.; Berman, J.; McKhann, G. M.; Patil, P. G.; et al. Subcallosal cingulate deep brain stimulation for treatment-resistant depression: a multisite, randomised, sham-controlled trial. *Lancet Psychiatry* **2017**, *4*, 839−849.
(28) Luo, Y.; Sun, Y.; Tian, X.; Zheng, X.; Wang, X.; Li, W.; Wu, X.; Shu, B.; Hou, W. Deep brain stimulation for Alzheimer's disease: stimulation parameters and potential mechanisms of action. *Front. Aging Neurosci.* **2021**, *13*, No. 619543.
(29) Bublitz, C.; Gilbert, F.; Soekadar, S. R. Concerns with the promotion of deep brain stimulation for obsessive−compulsive disorder. *Nat. Med.* **2023**, *29*, 18.
(30) Leinenga, G.; Langton, C.; Nisbet, R.; Götz, J. Ultrasound treatment of neurological diseases—current and emerging applications. *Nat. Rev. Neurol.* **2016**, *12*, 161−174.
(31) Meng, Y.; Hynynen, K.; Lipsman, N. Applications of focused ultrasound in the brain: from thermoablation to drug delivery. *Nat. Rev. Neurol.* **2021**, *17*, 7−22.
(32) Hallett, M. Transcranial magnetic stimulation: a primer. *Neuron* **2007**, *55*, 187−199.

https://doi.org/10.1021/acsnano.5c15238
ACS Nano XXXX, XXX, XXX−XXX

(33) Rossini, P. M.; Burke, D.; Chen, R.; Cohen, L. G.; Daskalakis, Z.; Di Iorio, R.; Di Lazzaro, V.; Ferreri, F.; Fitzgerald, P.; George, M. S.; et al. Non-invasive electrical and magnetic stimulation of the brain, spinal cord, roots and peripheral nerves: Basic principles and procedures for routine clinical and research application. An updated report from an IFCN Committee. *Clin. Neurophys.* **2015**, *126*, 1071−1107.
(34) Liu, A.; Vöröslakos, M.; Kronberg, G.; Henin, S.; Krause, M. R.; Huang, Y.; Opitz, A.; Mehta, A.; Pack, C. C.; Krekelberg, B.; et al. Immediate neurophysiological effects of transcranial electrical stimulation. *Nat. Commun.* **2018**, *9*, No. 5092.
(35) Polanía, R.; Nitsche, M. A.; Ruff, C. C. Studying and modifying brain function with non-invasive brain stimulation. *Nat. Neurosci.* **2018**, *21*, 174−187.
(36) Xu, S.; Wan, X.; Manshaii, F.; Che, Z.; Chen, J. Advances in Piezoelectric Nanogenerators for Self-Powered Cardiac Care. *Nano Trends* **2024**, *7*, No. 100042.
(37) Xu, S.; Manshaii, F.; Xiao, X.; Yin, J.; Chen, J. Triboelectric Nanogenerators for Self-Powered Neurostimulation. *Nano Res.* **2024**, *17*, 8926−8941.
(38) Weise, K.; Numssen, O.; Kalloch, B.; Zier, A. L.; Thielscher, A.; Haueisen, J.; Hartwigsen, G.; Knösche, T. R. Precise motor mapping with transcranial magnetic stimulation. *Nat. Protoc.* **2023**, *18*, 293−318.
(39) Buetefisch, C. M.; Wei, L.; Gu, X.; Epstein, C. M.; Yu, S. P. Neuroprotection of Low-Frequency Repetitive Transcranial Magnetic Stimulation after Ischemic Stroke in Rats. *Ann. Neurol.* **2023**, *93*, 336−347.
(40) Lefaucheur, J.-P.; Aleman, A.; Baeken, C.; Benninger, D. H.; Brunelin, J.; Di Lazzaro, V.; Filipović, S. R.; Grefkes, C.; Hasan, A.; Hummel, F. C.; et al. Evidence-based guidelines on the therapeutic use of repetitive transcranial magnetic stimulation (rTMS): An update (2014−2018). *Clin. Neurophys.* **2020**, *131*, 474−528.
(41) Grossman, N.; Bono, D.; Dedic, N.; Kodandaramaiah, S. B.; Rudenko, A.; Suk, H.-J.; Cassara, A. M.; Neufeld, E.; Kuster, N.; Tsai, L.-H.; et al. Noninvasive deep brain stimulation via temporally interfering electric fields. *Cell* **2017**, *169*, 1029−1041.
(42) Kim, S.; Jo, Y.; Kook, G.; Pasquinelli, C.; Kim, H.; Kim, K.; Hoe, H.-S.; Choe, Y.; Rhim, H.; Thielscher, A.; et al. Transcranial focused ultrasound stimulation with high spatial resolution. *Brain Stimul.* **2021**, *14*, 290−300.
(43) Wang, B.; Aberra, A. S.; Grill, W. M.; Peterchev, A. V. Responses of model cortical neurons to temporal interference stimulation and related transcranial alternating current stimulation modalities. *J. Neural Eng.* **2022**, *19*, No. 066047.
(44) von Conta, J.; Kasten, F. H.; Ćurčić-Blake, B.; Aleman, A.; Thielscher, A.; Herrmann, C. S. Interindividual variability of electric fields during transcranial temporal interference stimulation (tTIS). *Sci. Rep.* **2021**, *11*, No. 20357.
(45) Violante, I. R.; Alania, K.; Cassarà, A. M.; Neufeld, E.; Acerbo, E.; Carron, R.; Williamson, A.; Kurtin, D. L.; Rhodes, E.; Hampshire, A.; et al. Non-invasive temporal interference electrical stimulation of the human hippocampus. *Nat. Neurosci.* **2023**, *26*, 1994−2004.
(46) Grossman, N.; Okun, M. S.; Boyden, E. S. Translating temporal interference brain stimulation to treat neurological and psychiatric conditions. *JAMA Neurol.* **2018**, *75*, 1307−1308.
(47) Vosskuhl, J.; Strüber, D.; Herrmann, C. S. Non-invasive brain stimulation: a paradigm shift in understanding brain oscillations. *Front. Human Neurosci.* **2018**, *12*, 211.
(48) Grossman, N.; Bono, D.; Dedic, N.; Kodandaramaiah, S. B.; Rudenko, A.; Suk, H.-J.; Cassara, A. M.; Neufeld, E.; Kuster, N.; Tsai, L.-H.; et al. Noninvasive deep brain stimulation via temporally interfering electric fields. *Cell* **2017**, *169*, 1029−1041.
(49) Violante, I. R.; Alania, K.; Cassarà, A. M.; Neufeld, E.; Acerbo, E.; Carron, R.; Williamson, A.; Kurtin, D. L.; Rhodes, E.; Hampshire, A.; et al. Non-invasive temporal interference electrical stimulation of the human hippocampus. *Nat. Neurosci.* **2023**, *26*, 1994−2004.
(50) Wischnewski, M.; Tran, H.; Zhao, Z.; Shirinpour, S.; Haigh, Z. J.; Rotteveel, J.; Perera, N. D.; Alekseichuk, I.; Zimmermann, J.; Opitz, A. Induced neural phase precession through exogenous electric fields. *Nat. Commun.* **2024**, *15*, No. 1687.
(51) Meng, H.; Houston, M.; Dias, N.; Guo, C.; Francisco, G.; Zhang, Y.; Li, S. Efficacy of High-Definition Transcranial Alternating Current Stimulation (HD-tACS) at the M1 Hotspot Versus C3 Site in Modulating Corticospinal Tract Excitability. *Biomedicines* **2024**, *12*, 2635.
(52) Liu, X.; Qiu, F.; Hou, L.; Wang, X. Review of noninvasive or minimally invasive deep brain stimulation. *Front. Behav. Neurosci.* **2022**, *15*, No. 820017.
(53) Guo, W.; He, Y.; Zhang, W.; Sun, Y.; Wang, J.; Liu, S.; Ming, D. A novel non-invasive brain stimulation technique:"Temporally interfering electrical stimulation". *Front. Neurosci.* **2023**, *17*, No. 1092539.
(54) Neuling, T.; Ruhnau, P.; Weisz, N.; Herrmann, C. S.; Demarchi, G. Faith and oscillations recovered: On analyzing EEG/MEG signals during tACS. *NeuroImage* **2017**, *147*, 960−963.
(55) Minami, S.; Amano, K. Illusory jitter perceived at the frequency of alpha oscillations. *Curr. Biol.* **2017**, *27*, 2344−2351.
(56) Herrmann, C. S.; Strüber, D. What can transcranial alternating current stimulation tell us about brain oscillations? *Curr. Behav. Neurosci. Rep.* **2017**, *4*, 128−137.
(57) Sunshine, M. D.; Cassarà, A. M.; Neufeld, E.; Grossman, N.; Mareci, T. H.; Otto, K. J.; Boyden, E. S.; Fuller, D. D. Restoration of breathing after opioid overdose and spinal cord injury using temporal interference stimulation. *Commun. Biol.* **2021**, *4*, 107.
(58) Song, X.; Zhao, X.; Li, X.; Liu, S.; Ming, D. Multi-channel transcranial temporally interfering stimulation (tTIS): Application to living mice brain. *J. Neural Eng.* **2021**, *18*, No. 036003.
(59) Missey, F.; Rusina, E.; Acerbo, E.; Botzanowski, B.; Trébuchon, A.; Bartolomei, F.; Jirsa, V.; Carron, R.; Williamson, A. Orientation of temporal interference for non-invasive deep brain stimulation in epilepsy. *Front. Neurosci.* **2021**, *15*, No. 633988.
(60) Ma, R.; Xia, X.; Zhang, W.; Lu, Z.; Wu, Q.; Cui, J.; Song, H.; Fan, C.; Chen, X.; Zha, R.; et al. High gamma and beta temporal interference stimulation in the human motor cortex improves motor functions. *Front. Neurosci.* **2022**, *15*, No. 800436.
(61) Collavini, S.; Fernández-Corazza, M.; Oddo, S.; Princich, J. P.; Kochen, S.; Muravchik, C. H. Improvements on spatial coverage and focality of deep brain stimulation in pre-surgical epilepsy mapping. *J. Neural Eng.* **2021**, *18*, No. 046004.
(62) Su, X.; Guo, J.; Zhou, M.; Chen, J.; Li, L.; Chen, Y.; Sui, X.; Li, H.; Chai, X. Computational modeling of spatially selective retinal stimulation with temporally interfering electric fields. *IEEE Trans. Neural Syst. Rehabil. Eng.* **2021**, *29*, 418−428.
(63) Lee, J.; Park, E.; Kang, W.; Kim, Y.; Lee, K.-S.; Park, S.-M. An efficient noninvasive neuromodulation modality for overactive bladder using time interfering current method. *IEEE Trans. Biomed. Eng.* **2021**, *68*, 214−224.
(64) Liu, X.; Qi, S.; Hou, L.; Liu, Y.; Wang, X. Noninvasive deep brain stimulation via temporal interference electric fields enhanced motor performance of mice and its neuroplasticity mechanisms. *Mol. Neurobiol.* **2024**, *61*, 3314−3329.
(65) Botzanowski, B.; Donahue, M. J.; Ejneby, M. S.; Gallina, A. L.; Ngom, I.; Missey, F.; Acerbo, E.; Byun, D.; Carron, R.; Cassarà, A. M.; et al. Noninvasive Stimulation of Peripheral Nerves using Temporally-Interfering Electrical Fields. *Adv. Healthcare Mater.* **2022**, *11*, No. 2200075.
(66) Yang, C.; Xu, Y.; Feng, X.; Wang, B.; Du, Y.; Wang, K.; Lü, J.; Huang, L.; Qian, Z.; Wang, Z. Transcranial temporal interference stimulation of the right globus pallidus in Parkinson's disease. *Mov. Disord.* **2024**, 1061−1069, DOI: 10.1002/mds.29967.
(67) He, S.; West, T. O.; Plazas, F. R.; Wehmeyer, L.; Pogosyan, A.; Deli, A.; Wiest, C.; Herz, D. M.; Simpson, T. G.; Andrade, P. Cortico-thalamic tremor circuits and their associations with deep brain stimulation effects in essential tremor. *Brain* **2024**, *148*, No. awae387.
(68) Vassiliadis, P.; Beanato, E.; Popa, T.; Windel, F.; Morishita, T.; Neufeld, E.; Duque, J.; Derosiere, G.; Wessel, M. J.; Hummel, F. C. Non-invasive stimulation of the human striatum disrupts reinforce-

https://doi.org/10.1021/acsnano.5c15238
ACS Nano XXXX, XXX, XXX−XXX

ment learning of motor skills. *Nat. Human Behav.* **2024**, *8*, 1581−1598.
(69) Yatsuda, K.; Yu, W.; Gomez-Tames, J. Population-level insights into temporal interference for focused deep brain neuromodulation. *Front. Human Neurosci.* **2024**, *18*, No. 1308549.
(70) Ang, R.; Marina, N. Low-frequency oscillations in cardiac sympathetic neuronal activity. *Front. Physiol.* **2020**, *11*, No. 521675.
(71) Wessel, M. J.; Beanato, E.; Popa, T.; Windel, F.; Vassiliadis, P.; Menoud, P.; Beliaeva, V.; Violante, I. R.; Abderrahmane, H.; Dzialecka, P.; et al. Noninvasive theta-burst stimulation of the human striatum enhances striatal activity and motor skill learning. *Nat. Neurosci.* **2023**, *26*, 2005−2016.
(72) Beanato, E.; Moon, H.-J.; Windel, F.; Vassiliadis, P.; Wessel, M. J.; Popa, T.; Pauline, M.; Neufeld, E.; De Falco, E.; Gauthier, B.; et al. Noninvasive modulation of the hippocampal-entorhinal complex during spatial navigation in humans. *Sci. Adv.* **2024**, *10*, No. eado4103.
(73) Qi, S.; Liu, X.; Yu, J.; Liang, Z.; Liu, Y.; Wang, X. Temporally interfering electric fields brain stimulation in primary motor cortex of mice promotes motor skill through enhancing neuroplasticity. *Brain Stimul.* **2024**, *17*, 245−257.
(74) Lim, Y.-S.; Kim, J. H.; Kim, J.; Hoang, M.; Kang, W.; Koh, M.; Choi, W. H.; Park, S.; Jeong, U.; Kim, D. H.; Park, S. M. Precise control of tibial nerve stimulation for bladder regulation via evoked compound action potential feedback mechanisms. *Nat. Commun.* **2025**, *16*, No. 4115.
(75) Radman, T.; Ramos, R. L.; Brumberg, J. C.; Bikson, M. Role of cortical cell type and morphology in subthreshold and suprathreshold uniform electric field stimulation in vitro. *Brain Stimul.* **2009**, *2*, 215−228.
(76) DeLong, M. R.; Wichmann, T. Basal ganglia circuits as targets for neuromodulation in Parkinson disease. *JAMA Neurol.* **2015**, *72*, 1354−1360.
(77) Aberra, A. S.; Wang, B.; Grill, W. M.; Peterchev, A. V. Simulation of transcranial magnetic stimulation in head model with morphologically-realistic cortical neurons. *Brain Stimul.* **2020**, *13*, 175−189.
(78) Caldas-Martinez, S.; Goswami, C.; Forssell, M.; Cao, J.; Barth, A. L.; Grover, P. Cell-specific effects of temporal interference stimulation on cortical function. *Commun. Biol.* **2024**, *7*, 1076.
(79) Benavides-Piccione, R.; Regalado-Reyes, M.; Fernaud-Espinosa, I.; Kastanauskaite, A.; Tapia-González, S.; León-Espinosa, G.; Rojo, C.; Insausti, R.; Segev, I.; DeFelipe, J. Differential structure of hippocampal CA1 pyramidal neurons in the human and mouse. *Cereb. Cortex* **2020**, *30*, 730−752.
(80) Major, G.; Larkum, M. E.; Schiller, J. Active properties of neocortical pyramidal neuron dendrites. *Annu. Rev. Neurosci.* **2013**, *36*, 1−24.
(81) Peng, Y.-R.; He, S.; Marie, H.; Zeng, S.-Y.; Ma, J.; Tan, Z.-J.; Lee, S. Y.; Malenka, R. C.; Yu, X. Coordinated changes in dendritic arborization and synaptic strength during neural circuit development. *Neuron* **2009**, *61*, 71−84.
(82) Jarsky, T.; Roxin, A.; Kath, W. L.; Spruston, N. Conditional dendritic spike propagation following distal synaptic activation of hippocampal CA1 pyramidal neurons. *Nat. Neurosci.* **2005**, *8*, 1667−1676.
(83) Otomo, K.; Perkins, J.; Kulkarni, A.; Stojanovic, S.; Roeper, J.; Paladini, C. A. In vivo patch-clamp recordings reveal distinct subthreshold signatures and threshold dynamics of midbrain dopamine neurons. *Nat. Commun.* **2020**, *11*, No. 6286.
(84) Becker, L. A.; Li, B.; Priebe, N. J.; Seidemann, E.; Taillefumier, T. Exact analysis of the subthreshold variability for conductance-based neuronal models with synchronous synaptic inputs. *Phys. Rev. X* **2024**, *14*, No. 011021.
(85) Mirzakhalili, E.; Barra, B.; Capogrosso, M.; Lempka, S. F. Biophysics of temporal interference stimulation. *Cell Syst.* **2020**, *11*, 557−572.
(86) Nakamura, Y.; Kurabe, M.; Matsumoto, M.; Sato, T.; Miyashita, S.; Hoshina, K.; Kamiya, Y.; Tainaka, K.; Matsuzawa, H.; Ohno, N.; Ueno, M. Cerebrospinal fluid-contacting neuron tracing reveals structural and functional connectivity for locomotion in the mouse spinal cord. *eLife* **2023**, *12*, No. e83108.
(87) Zhao, X.; Zhou, Y.; Song, Y.; Xu, J.; Li, J.; Tat, T.; Chen, G.; Li, S.; Chen, J. Permanent Fluidic Magnets for Liquid Bioelectronics. *Nat. Mater.* **2024**, *23*, 703−710.
(88) Zhou, Y.; Zhao, X.; Xu, J.; Fang, Y.; Chen, G.; Song, Y.; Li, S.; Chen, J. Giant magnetoelastic effect in soft systems for bioelectronics. *Nat. Mater.* **2021**, *20*, 1670−1676.
(89) Budde, R. B.; Williams, M. T.; Irazoqui, P. P. Temporal interference current stimulation in peripheral nerves is not driven by envelope extraction. *J. Neural Eng.* **2023**, *20*, No. 026041.
(90) Mirzakhalili, E.; Barra, B.; Capogrosso, M.; Lempka, S. F. Biophysics of temporal interference stimulation. *Cell Syst.* **2020**, *11*, 557−572.
(91) Vieira, P. G.; Krause, M. R.; Pack, C. C. Temporal interference stimulation disrupts spike timing in the primate brain. *Nat. Commun.* **2024**, *15*, No. 4558.
(92) Varró, A.; Tomek, J.; Nagy, N.; Virág, L.; Passini, E.; Rodriguez, B.; Baczkó, I. Cardiac transmembrane ion channels and action potentials: cellular physiology and arrhythmogenic behavior. *Physiol. Rev.* **2021**, *101*, 1083−1176.
(93) Esmaeilpour, Z.; Kronberg, G.; Reato, D.; Parra, L. C.; Bikson, M. Temporal interference stimulation targets deep brain regions by modulating neural oscillations. *Brain Stimul.* **2021**, *14*, 55−65.
(94) Pitt, G. S.; Matsui, M.; Cao, C. Voltage-gated calcium channels in nonexcitable tissues. *Annu. Rev. Physiol.* **2021**, *83*, 183−203.
(95) Goodwin, G.; McMahon, S. B. The physiological function of different voltage-gated sodium channels in pain. *Nat. Rev. Neurosci.* **2021**, *22*, 263−274.
(96) Qiao, J.; Xu, X.; Zhou, X.; Wu, Y.; Wang, J.; Xi, H.; Liu, C.; Wang, Y.; Zhou, L.; Zhou, X.; et al. Targeted ganglion delivery of CaV2. 2-mediated peptide by DNA nanoflowers for relieving myocardial infarction and neuropathic pain. *ACS Nano* **2025**, *19*, 13037−13052.
(97) Vasu, S. O.; Kaphzan, H. The role of sodium channels in direct current stimulation—axonal perspective. *Cell Rep.* **2021**, *37*, 109832 DOI: 10.1016/j.celrep.2021.109832.
(98) Benarroch, J. M.; Asally, M. The microbiologist's guide to membrane potential dynamics. *Trends Microbiol.* **2020**, *28*, 304−314.
(99) Middleton, J. W.; Longtin, A.; Benda, J.; Maler, L. The cellular basis for parallel neural transmission of a high-frequency stimulus and its low-frequency envelope. *Proc. Natl. Acad. Sci. U.S.A.* **2006**, *103*, 14596−14601.
(100) Jitnumsab, T.; Yambangyang, P. Validation of Temporal Interference Stimulation with Steamed Flour-Based Phantoms in Spinal Cord Neuromodulation. In *IEEE Biomed. Eng. Int. Conf.*; IEEE: Tokyo, Japan, 2023; pp 1−5.
(101) Lee, S.; Park, J.; Choi, D. S.; Lee, C.; Lee, C.; Im, C.-H. Multipair transcranial temporal interference stimulation for improved focalized stimulation of deep brain regions: A simulation study. *Comput. Biol. Med.* **2022**, *143*, No. 105337.
(102) Wang, Y.; Jiang, Z.; Chu, C.; Zhang, Z.; Wang, J.; Li, D.; He, N.; Fietkiewicz, C.; Zhou, C.; Kaiser, M.; et al. Push-pull effects of basal ganglia network in Parkinson's disease inferred by functional MRI. *npj Parkin. Dis.* **2024**, *10*, 224.
(103) Zibandepour, M.; Shojaei, A.; Larki, A. A.; Delrobaei, M. Preliminary Guidelines for Electrode Positioning in Noninvasive Deep Brain Stimulation via Temporally Interfering Electric Fields. In *IEEE Proc. RSI Int. Conf. Robot. Mech.*; IEEE: Tehran, Iran, 2023; pp 739−744.
(104) Forró, C.; Musall, S.; Montes, V. R.; Linkhorst, J.; Walter, P.; Wessling, M.; Offenhäusser, A.; Ingebrandt, S.; Weber, Y.; Lampert, A.; Santoro, F. Toward the Next Generation of Neural Iontronic Interfaces. *Adv. Healthcare Mater.* **2023**, *12*, No. 2301055.
(105) Jenkins, E. P. W.; Finch, A.; Gerigk, M.; Triantis, I. F.; Watts, C.; Malliaras, G. G. Electrotherapies for glioblastoma. *Adv. Sci.* **2021**, *8*, No. 2100978.
(106) Dres, M.; de Abreu, M. G.; Merdji, H.; Müller-Redetzky, H.; Dellweg, D.; Randerath, W. J.; Mortaza, S.; Jung, B.; Bruells, C.;

https://doi.org/10.1021/acsnano.5c15238
ACS Nano XXXX, XXX, XXX−XXX

Moerer, O.; et al. Randomized clinical study of temporary transvenous phrenic nerve stimulation in difficult-to-wean patients. *Am. J. Respir. Crit. Care Med.* **2022**, *205*, 1169−1178.
(107) Karimi, F.; Attarpour, A.; Amirfattahi, R.; Nezhad, A. Z. Computational analysis of non-invasive deep brain stimulation based on interfering electric fields. *Phys. Med. Biol.* **2019**, *64*, No. 235010.
(108) Esmaeilpour, Z.; Kronberg, G.; Reato, D.; Parra, L. C.; Bikson, M. Temporal interference stimulation targets deep brain regions by modulating neural oscillations. *Brain Stimul.* **2021**, *14*, 55−65.
(109) Luff, C. E.; Dzialecka, P.; Acerbo, E.; Williamson, A.; Grossman, N. Pulse-width modulated temporal interference (PWM-TI) brain stimulation. *Brain Stimul.* **2024**, *17*, 92−103.
(110) Bahn, S.; Lee, C.; Kang, B. Y. A computational study on the optimization of transcranial temporal interfering stimulation with high-definition electrodes using unsupervised neural networks. *Hum. Brain Map.* **2023**, *44*, 1829−1845.
(111) Nasr, K.; Haslacher, D.; Dayan, E.; Censor, N.; Cohen, L. G.; Soekadar, S. R. Breaking the boundaries of interacting with the human brain using adaptive closed-loop stimulation. *Prog. Neurobiol.* **2022**, *216*, No. 102311.
(112) Fani, N.; Treadway, M. T. Potential applications of temporal interference deep brain stimulation for the treatment of trans-diagnostic conditions in psychiatry. *Neuropsychopharmacology* **2024**, *49*, 305−306.
(113) Sun, Y.; Shen, A.; Du, C.; Sun, J.; Chen, X.; Gao, X. A Real-Time Non-Implantation Bi-Directional Brain-Computer Interface Solution without Stimulation Artifacts. *IEEE Trans. Neural Syst. Rehabil. Eng.* **2023**, *31*, 3566−3575.
(114) Busch, J. L.; Kaplan, J.; Habets, J. G.; Feldmann, L. K.; Roediger, J.; Köhler, R. M.; Merk, T.; Faust, K.; Schneider, G.-H.; Bergman, H.; et al. Single threshold adaptive deep brain stimulation in Parkinson's disease depends on parameter selection, movement state and controllability of subthalamic beta activity. *Brain Stimul.* **2024**, *17*, 125−133.
(115) Tuck, M.; Blanc, L.; Touti, R.; Patterson, N. H.; Van Nuffel, S.; Villette, S.; Taveau, J.-C.; Römpp, A.; Brunelle, A.; Lecomte, S.; Desbenoit, N. Multimodal imaging based on vibrational spectroscopies and mass spectrometry imaging applied to biological tissue: a multiscale and multiomics review. *Anal. Chem.* **2021**, *93*, 445−477.
(116) McGlynn, E.; Nabaei, V.; Ren, E.; Galeote-Checa, G.; Das, R.; Curia, G.; Heidari, H. The future of neuroscience: flexible and wireless implantable neural electronics. *Adv. Sci.* **2021**, *8*, No. 2002693.
(117) Nocon, J. C.; Gritton, H. J.; James, N. M.; Mount, R. A.; Qu, Z.; Han, X.; Sen, K. Parvalbumin neurons enhance temporal coding and reduce cortical noise in complex auditory scenes. *Commun. Biol.* **2023**, *6*, 751.
(118) Zhou, Y.; Zhao, X.; Xu, J.; Chen, G.; Tat, T.; Li, J.; Chen, J. A multimodal magnetoelastic artificial skin for underwater haptic sensing. *Sci. Adv.* **2024**, *10*, No. eadj8567.
(119) Xu, S.; Xiao, X.; Manshaii, F.; Chen, J. Injectable fluorescent neural interfaces for cell-specific stimulating and imaging. *Nano Lett.* **2024**, *24*, 4703−4716.
(120) Wang, Y.; Beeraka, N. M.; Zhu, Y.; Ge, M.; Nikolenko, V. N.; Xu, S. Can Optogenetics Decode Human-Specific Hyperexcitability Circuits? *Med. Mat* **2025**, *2*, 140−144.
(121) Wang, Y.; Ge, M.; Wang, J.; Xu, Y.; Wang, N.; Xu, S. Metabolic reprogramming in ischemic stroke: when glycolytic overdrive meets lipid storm. *Cell Death Dis.* **2025**, *16*, 788 DOI: 10.1038/s41419-025-08114-w.
(122) Ligresti, A.; De Petrocellis, L.; Di Marzo, V. From phytocannabinoids to cannabinoid receptors and endocannabinoids: pleiotropic physiological and pathological roles through complex pharmacology. *Physiol. Rev.* **2016**, *96*, 1593−1659.
(123) Leppik, L.; Zhihua, H.; Mobini, S.; Thottakkattumana Parameswaran, V.; Eischen-Loges, M.; Slavici, A.; Helbing, J.; Pindur, L.; Oliveira, K. M.; Bhavsar, M. B.; et al. Combining electrical stimulation and tissue engineering to treat large bone defects in a rat model. *Sci. Rep.* **2018**, *8*, No. 6307.
(124) Colon, E.; Liberati, G.; Mouraux, A. EEG frequency tagging using ultra-slow periodic heat stimulation of the skin reveals cortical activity specifically related to C fiber thermonociceptors. *NeuroImage* **2017**, *146*, 266−274.
(125) Jabban, L.; Routledge, N.; Hadjigeorgiou, N.; Hoyle, A.; Graham-Harper-Cater, J.; Zhang, D.; Metcalfe, B. W. The comfort of temporal interference stimulation on the forearm: computational and psychophysical evaluation. *J. Neural Eng.* **2025**, *22*, No. 026044.
(126) Gulyaev, Y. V.; Markov, A.; Koreneva, L.; Zakharov, P. Dynamical infrared thermography in humans. *IEEE Eng. Med. Biol. Magaz.* **1995**, *14*, 766−771.
(127) Mohammadi, L.; Behnam, H.; Tavakkoli, J.; Avanaki, M. R. Skull's photoacoustic attenuation and dispersion modeling with deterministic ray-tracing: Towards real-time aberration correction. *Sensors* **2019**, *19*, 345.
(128) Jellinger, K. A. Recent update on the heterogeneity of the Alzheimer's disease spectrum. *J. Neural Transmis.* **2022**, *129*, 1−24.
(129) Jung, N. Y.; Park, C. K.; Kim, M.; Lee, P. H.; Sohn, Y. H.; Chang, J. W. The efficacy and limits of magnetic resonance−guided focused ultrasound pallidotomy for Parkinson's disease: a Phase I clinical trial. *J. Neurosurg.* **2019**, *130*, 1853−1861.
(130) Oehrn, C. R.; Cernera, S.; Hammer, L. H.; Shcherbakova, M.; Yao, J.; Hahn, A.; Wang, S.; Ostrem, J. L.; Little, S.; Starr, P. A. Chronic adaptive deep brain stimulation versus conventional stimulation in Parkinson's disease: a blinded randomized feasibility trial. *Nat. Med.* **2024**, *30*, 3345−3356.
(131) Zich, C.; Debener, S.; Kranczioch, C.; Bleichner, M. G.; Gutberlet, I.; De Vos, M. Real-time EEG feedback during simultaneous EEG−fMRI identifies the cortical signature of motor imagery. *NeuroImage* **2015**, *114*, 438−447.
(132) Munn, B. R.; Müller, E. J.; Medel, V.; Naismith, S. L.; Lizier, J. T.; Sanders, R. D.; Shine, J. M. Neuronal connected burst cascades bridge macroscale adaptive signatures across arousal states. *Nat. Commun.* **2023**, *14*, No. 6846.
(133) Shahsavarani, S.; Thibodeaux, D. N.; Xu, W.; Kim, S. H.; Lodgher, F.; Nwokeabia, C.; Cambareri, M.; Yagielski, A. J.; Zhao, H. T.; Handwerker, D. A.; et al. Cortex-wide neural dynamics predict behavioral states and provide a neural basis for resting-state dynamic functional connectivity. *Cell Rep.* **2023**, *42*, No. 112527.
(134) Boehm, K. M.; Khosravi, P.; Vanguri, R.; Gao, J.; Shah, S. P. Harnessing multimodal data integration to advance precision oncology. *Nat. Rev. Cancer* **2022**, *22*, 114−126.
(135) Wang, Y.; Ge, M.; Wang, R.; Zhu, Y.; Xu, S. Injectable Ultrasonic Metagels for Intracranial Monitoring. *npj Biosens.* **2025**, *2*, 38 DOI: 10.1038/s44328-025-00058-7.
(136) Xu, S.; Ge, M.; Chen, S.; Wang, Y.; Tang, Y.; Wang, J.; Cui, X.; Sun, C.; Zeng, H.; Wang, N.; et al. Leveraging Laser-Patterned Copper Electrodes for Personal Healthcare. *Small Methods* **2025**, *35*, No. e00056.
(137) Wang, Y.; Tang, Y.; Wang, Q.; Ge, M.; Wang, J.; Cui, X.; Wang, N.; Bao, Z.; Chen, S.; Wang, J.; Xu, S. Advances in brain computer interface for amyotrophic lateral sclerosis communication. *Brain-X* **2025**, *3*, No. e70023.
(138) Corbett, A.; Williams, G.; Creese, B.; Hampshire, A.; Hayman, V.; Palmer, A.; Filakovszky, A.; Mills, K.; Cummings, J.; Aarsland, D.; et al. Cognitive decline in older adults in the UK during and after the COVID-19 pandemic: a longitudinal analysis of PROTECT study data. *Lancet Healthy Longev.* **2023**, *4*, e591−e599.
(139) Zhang, Z.; Lin, B.-S.; Wu, C.-W. G.; Hsieh, T.-H.; Liou, J.-C.; Li, Y.-T.; Peng, C.-W. Designing and pilot testing a novel transcranial temporal interference stimulation device for neuromodulation. *IEEE Trans. Neural Syst. Rehabil. Eng.* **2022**, *30*, 1483−1493.
(140) Sarica, C.; Iorio-Morin, C.; Aguirre-Padilla, D. H.; Najjar, A.; Paff, M.; Fomenko, A.; Yamamoto, K.; Zemmar, A.; Lipsman, N.; Ibrahim, G. M.; et al. Implantable pulse generators for deep brain stimulation: challenges, complications, and strategies for practicality and longevity. *Front. Hum. Neurosci.* **2021**, *15*, No. 708481.

https://doi.org/10.1021/acsnano.5c15238
ACS Nano XXXX, XXX, XXX−XXX

(141) Cehajic-Kapetanovic, J.; Singh, M. S.; Zrenner, E.; MacLaren, R. E. Bioengineering strategies for restoring vision. *Nat. Biomed. Eng.* **2023**, *7*, 387−404.
(142) Bergmann, T. O.; Hartwigsen, G. Inferring causality from noninvasive brain stimulation in cognitive neuroscience. *J. Cogn. Neurosci.* **2021**, *33*, 195−225.
(143) Zheng, Z.; Li, G.; Cui, C.; Wang, F.; Wang, X.; Xu, Z.; Guo, H.; Chen, Y.; Tang, H.; Wang, D.; et al. Preventing autosomal-dominant hearing loss in Bth mice with CRISPR/CasRx-based RNA editing. *Signal Transduct. Target. Ther.* **2022**, *7*, 79.
(144) Pozdniakov, I.; Vorobiova, A. N.; Galli, G.; Rossi, S.; Feurra, M. Online and offline effects of transcranial alternating current stimulation of the primary motor cortex. *Sci. Rep.* **2021**, *11*, No. 3854.
(145) Huang, Y. Visualizing interferential stimulation of human brains. *Front. Hum. Neurosci.* **2023**, *17*, No. 1239114.
(146) Shan, Y.; Wang, H.; Yang, Y.; Wang, J.; Zhao, W.; Huang, Y.; Wang, H.; Han, B.; Pan, N.; Jin, X.; et al. Evidence of a large current of transcranial alternating current stimulation directly to deep brain regions. *Mol. Psychiatry* **2023**, *28*, 5402−5410.
(147) Collavini, S.; Fernández-Corazza, M.; Oddo, S.; Princich, J. P.; Kochen, S.; Muravchik, C. H. Improvements on spatial coverage and focality of deep brain stimulation in pre-surgical epilepsy mapping. *J. Neural Eng.* **2021**, *18*, No. 046004.
(148) Wang, H.; Shi, Z.; Sun, W.; Zhang, J.; Wang, J.; Shi, Y.; Yang, R.; Li, C.; Chen, D.; Wu, J.; et al. Development of a non-invasive deep brain stimulator with precise positioning and real-time monitoring of bioimpedance. *Front. Neuroinform.* **2020**, *14*, No. 574189.
(149) Nielsen, J. D.; Madsen, K. H.; Puonti, O.; Siebner, H. R.; Bauer, C.; Madsen, C. G.; Saturnino, G. B.; Thielscher, A. Automatic skull segmentation from MR images for realistic volume conductor models of the head: Assessment of the state-of-the-art. *NeuroImage* **2018**, *174*, 587−598.
(150) Lindgren, N.; Henningsen, M. J.; Jacobsen, C.; Villa, C.; Kleiven, S.; Li, X. Prediction of skull fractures in blunt force head traumas using finite element head models. *Biomechan. Model. Mechanobiol.* **2024**, *23*, 207−225.
(151) Khalifa, A.; Abrishami, S. M.; Zaeimbashi, M.; Tang, A. D.; Coughlin, B.; Rodger, J.; Sun, N. X.; Cash, S. S. Magnetic temporal interference for noninvasive and focal brain stimulation. *J. Neural Eng.* **2023**, *20*, No. 016002.
(152) Budde, R. B.; Williams, M. T.; Irazoqui, P. P. Temporal interference current stimulation in peripheral nerves is not driven by envelope extraction. *J. Neural Eng.* **2023**, *20*, No. 026041.
(153) Verma, N.; Graham, R. D.; Mudge, J.; Trevathan, J. K.; Franke, M.; Shoffstall, A. J.; Williams, J.; Dalrymple, A. N.; Fisher, L. E.; Weber, D. J.; et al. Augmented transcutaneous stimulation using an injectable electrode: A computational study. *Front. Bioeng. Biotechnol.* **2021**, *9*, No. 796042.
(154) Zhu, X.; Li, Y.; Zheng, L.; Shao, B.; Liu, X.; Li, C.; Huang, Z.-G.; Liu, T.; Wang, J. Multi-point temporal interference stimulation by using each electrode to carry different frequency currents. *IEEE Access* **2019**, *7*, 168839−168848.
(155) Goswami, C.; Grover, P. Automated Electrical Waveform Design for Cell-Type Selective Stimulation. In *IEEE/EMBS Conf. Neural Eng.*; IEEE: Baltimore, USA, 2023; pp 1−6.
(156) Rosa, B. M. G.; Yang, G. Z. Bladder volume monitoring using electrical impedance tomography with simultaneous multi-tone tissue stimulation and DFT-based impedance calculation inside an FPGA. *IEEE Trans. Biomed. Circuits Syst.* **2020**, *14*, 775−786.
(157) Chen, G.; Zhang, X.; Zhang, J.; Li, F.; Duan, S. A novel brain-computer interface based on audio-assisted visual evoked EEG and spatial-temporal attention CNN. *Front. Neurorobot.* **2022**, *16*, No. 995552.
(158) Che, Z.; Wan, X.; Xu, J.; Duan, C.; Zheng, T.; Chen, J. Speaking without vocal folds using a machine-learning-assisted wearable sensing-actuation system. *Nat. Commun.* **2024**, *15*, No. 1873.
(159) Xiao, X.; Yin, J.; Xu, J.; Tat, T.; Chen, J. Advances in machine learning for wearable sensors. *ACS Nano* **2024**, *18*, 22734−22751.
(160) Xu, S.; Manshaii, F.; Xiao, X.; Chen, J. Artificial intelligence assisted nanogenerator applications. *J. Mater. Chem. A* **2025**, *13*, 832−854.
(161) Yan, Y.; Dahmani, L.; Ren, J.; Shen, L.; Peng, X.; Wang, R.; He, C.; Jiang, C.; Gong, C.; Tian, Y.; et al. Reconstructing lost BOLD signal in individual participants using deep machine learning. *Nat. Commun.* **2020**, *11*, No. 5046.
(162) Islam, S.; Aziz, M. T.; Nabil, H. R.; Jim, J. R.; Mridha, M. F.; Kabir, M. M.; Asai, N.; Shin, J. Generative adversarial networks (GANs) in medical imaging: Advancements, applications, and challenges. *IEEE Access* **2024**, *12*, 35728−35753.
(163) Boopathy, P.; Liyanage, M.; Deepa, N.; Velavali, M.; Reddy, S.; Maddikunta, P. K. R.; Khare, N.; Gadekallu, T. R.; Hwang, W.-J.; Pham, Q.-V. Deep learning for intelligent demand response and smart grids: A comprehensive survey. *Comput. Sci. Rev.* **2024**, *51*, No. 100617.
(164) López-García, D.; Sobrado, A.; Peñalver, J. M.; Górriz, J. M.; Ruz, M. Multivariate pattern analysis techniques for electro-encephalography data to study flanker interference effects. *Int. J. Neural Syst.* **2020**, *30*, No. 2050024.
(165) Stoupis, D.; Samaras, T. Non-invasive stimulation with temporal interference: optimization of the electric field deep in the brain with the use of a genetic algorithm. *J. Neural Eng.* **2022**, *19*, No. 056018.
(166) Zideh, M. J.; Chatterjee, P.; Srivastava, A. K. Physics-informed machine learning for data anomaly detection, classification, localization, and mitigation: A review, challenges, and path forward. *IEEE Access* **2024**, *12*, 4597−4617.
(167) Vassiliadis, P.; Stiennon, E.; Windel, F.; Wessel, M. J.; Beanato, E.; Hummel, F. C. Safety, tolerability and blinding efficiency of non-invasive deep transcranial temporal interference stimulation: first experience from more than 250 sessions. *J. Neural Eng.* **2024**, *21*, No. 024001.
(168) Wang, X.; Zwosta, K.; Hennig, J.; Böhm, I.; Ehrlich, S.; Wolfensteller, U.; Ruge, H. The dynamics of functional brain network segregation in feedback-driven learning. *Commun. Biol.* **2024**, *7*, 531.
(169) Wang, B.; Aberra, A. S.; Grill, W. M.; Peterchev, A. V. Responses of model cortical neurons to temporal interference stimulation and related transcranial alternating current stimulation modalities. *J. Neural Eng.* **2022**, *19*, No. 066047.
(170) Luff, C. E.; Dzialecka, P.; Acerbo, E.; Williamson, A.; Grossman, N. Pulse-width modulated temporal interference (PWM-TI) brain stimulation. *Brain Stimul.* **2024**, *17*, 92−103.
(171) Xu, S.; Manshaii, F.; Chen, J. Multiphasic interfaces enabled aero-elastic capacitive pressure sensors. *Matter* **2024**, *7*, 2351−2354.
(172) Yin, J.; Wang, S.; Tat, T.; Chen, J. Motion artefact management for soft bioelectronics. *Nat. Rev. Bioeng.* **2024**, *2*, 541−558.
(173) Zhang, H.; Zhu, M.; Jiang, Y.; Wang, D.; Wang, X.; Yang, Z.; Huang, W.; Chen, S.; Li, G. A Robust Extraction Approach of Auditory Brainstem Response Using Adaptive Kalman Filtering Method. *IEEE Trans. Biomed. Eng.* **2022**, *69*, 3792−3802.
(174) Khalifa, A.; Abrishami, S. M.; Zaeimbashi, M.; Tang, A. D.; Coughlin, B.; Rodger, J.; Sun, N. X.; Cash, S. S. Magnetic temporal interference for noninvasive and focal brain stimulation. *J. Neural Eng.* **2023**, *20*, No. 016002.
(175) Liu, R.; Ma, R.; Liu, X.; Zhou, X.; Wang, X.; Yin, T.; Liu, Z. A noninvasive deep brain stimulation method via temporal-spatial interference magneto-acoustic effect: simulation and experimental validation. *IEEE Trans. Ultrason., Ferroelec. Freq. Control* **2022**, *69*, 2474−2483.
(176) Zijlmans, M.; Zweiphenning, W.; Van Klink, N. Changing concepts in presurgical assessment for epilepsy surgery. *Nat. Rev. Neurol.* **2019**, *15*, 594−606.
(177) Ma, R.; Xia, X.; Zhang, W.; Lu, Z.; Wu, Q.; Cui, J.; Song, H.; Fan, C.; Chen, X.; Zha, R.; et al. High gamma and beta temporal interference stimulation in the human motor cortex improves motor functions. *Front. Neurosci.* **2022**, *15*, No. 800436.

https://doi.org/10.1021/acsnano.5c15238
ACS Nano XXXX, XXX, XXX−XXX